



**REVIEW OF AERONAUTICAL FATIGUE INVESTIGATIONS
IN POLAND
DURING THE PERIOD MAY 2011 TO MARCH 2013**

by
Dr Antoni Niepokólczycki
Institute of Aviation, Warsaw, POLAND

For Presentation at the 33 Conference of
the International Committee on Aeronautical Fatigue and Structural Integrity
Jerusalem, Israel, June 3-4, 2013

Approved for Public Release

CONTENTS

1. INTRODUCTION.....	3
2. AIRPLANE STRUCTURES AND MATERIALS TESTING	4
2.1 Full Scale Fatigue Test of New Undercarriage for Commuter Aircraft.....	4
2.2 Airworthiness Tests of the UAV Structure - Fatigue Issues	9
2.3 Recent Progress in Full Scale Fatigue Test of Pzl-130 "Orlik" TC-II Structure.....	19
2.4 Preliminary Verification of Selected Solutions for Crack Detection	23
2.5 Introduction of Fatigue Markers in Full Scale Fatigue Test of an Aircraft Structure	28
2.6 Numerical Simulation of Fatigue Fracture of the Turbine Disc.....	29
3. NON-DESTRUCTIVE TESTS AND STRUCTURAL HEALTH MONITORING	32
3.1 Damage Detection and Size Quantification of FML with the Use of NDE	32
3.2 The MMM Expert System: From a Reference Signal to the Method Validation	36
3.3 X-ray Diffraction Measurements for Riveted Joints - the Application of a Novel Methodology	38
4. JOINTS.....	39
4.1 Investigations into the Durability of Epoxy-Bonded Joints	39
4.2 The Influence of the Degree of the Rivet Hole Sizing on the Fatigue Life	41
4.3 Numerical Analysis of Material and Manufacturing Factors in Riveted Joints under the IMPERJA Project.....	42
4.4 Riveted Lap Joints in Aircraft Fuselage. Design, Analysis and Properties.....	43
4.5 Experimental and Numerical Analysis of the Rivet Installation Process.....	44
4.6 Fatigue Crack Location and fatigue life for riveted lap joints in aircraft fuselage	46
4.7 An Experimental Investigation on Crack Paths and Fatigue Behaviour of Riveted Lap Joints in Aircraft Fuselage.....	46
4.8 Analysis of the Quasi-Static Riveting Process for 90° Countersunk Rivet.....	49
5. IMPORTANT PUBLICATIONS.....	50

1. INTRODUCTION

This review gives the summary of work performed in Poland in the area of aeronautical fatigue during the period from May 2011 to March 2013.

The various contributions to this review come from the following sources:

Air Force Institute of Technology, Warsaw;
Warsaw University of Technology, Warsaw;
Military University of Technology, Warsaw;
Rzeszow University of Technology, Rzeszow;
AGH University of Science and Technology, Krakow
PZL – Mielec;
Institute of Aviation, Warsaw;

The names of the principal investigators and their affiliations are presented in brackets at the end of each chapter.

Full addresses of contributors are available through the author of this review at:

Antoni NIEPOKÓLCZYCKI
Institute of Aviation
Al. Krakowska 110/114
02-256 Warsaw, POLAND

Phone: (+48 22) 846 08 01 ext. 546

Mobile: +48 695 905 440

Fax: (+48 22) 846 75 36

E-mail: antekn@ilot.edu.pl

2. AIRPLANE STRUCTURES AND MATERIALS TESTING

2.1 Full Scale Fatigue Test of New Undercarriage for Commuter Aircraft

In order to establish the service life of the new main landing gear for the PZL M28 aircraft, the Full Scale Fatigue Test was performed at the test laboratory of Polskie Zakłady Lotnicze Sp. z o.o. in Mielec. The landing gear (see Fig. 1) was designed for operation on prepared and unprepared airfields. Maximum take-off and landing weight of the PZL M28, which is certified in commuter category, is 7500 kg (16535 lbs.). The undercarriage is of a fixed, tricycle type.

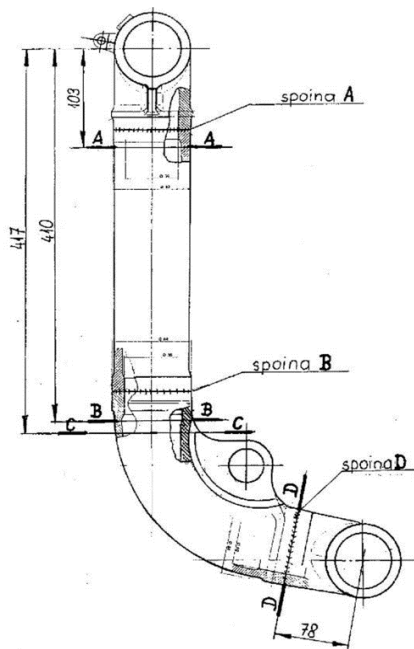


Fig. 1. The new main landing gear of PZL M28 aircraft

The main landing gear is of an articulating type with a braked wheel. It is mounted at the ends of the main landing gear beam, which is part of the fuselage structure. The main parts of the

landing gear are:

- leg – see Fig.2;
- oleo-pneumatic shock absorber – see Fig. 3;
- wheel axle;
- wheel with a brake.



The leg and shock absorber structure is made of high tensile strength low alloy steel 4330V – see Table 1 for chemical composition and Table 2 for mechanical properties. The leg consists of three parts welded using the electron beam welding method.

Fig. 2. The leg of the new landing gear

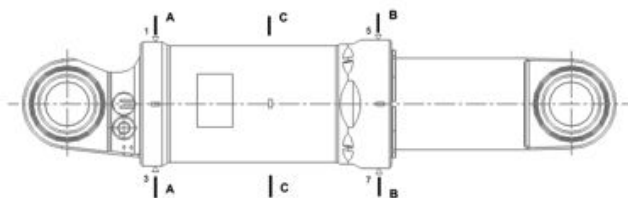


Fig. 3. The oleo-pneumatic shock absorber of the new landing gear

Table 1. Chemical composition of 4330V steel

C [%]	Si [%]	Mn [%]	P _{max} [%]	S _{max} [%]	Cr [%]	Ni [%]	V [%]
0.30÷0.34	0.15÷0.35	0.75÷1.00	0.025	0.010	0.75÷1.00	1.65÷2.00	0.05÷0.10

Table 2. Heat treatment conditions and tensile properties of 4330V steel

Heat treatment conditions	Ultimate tensile strength F _{tu} [MPa]
I. Normalize at 871÷927°C, air cool. II. Austenitize at 843÷871°C, oil quench. III. Tempering at 260÷371°C.	1517÷1655

Note: For longitudinal direction, for F_{tu} = 1559 MPa, 0.2% yield strength is 1297 MPa, elongation 13.0%, and cross section reduction 58.3%.

The main landing gear fatigue test was performed at the structural tests laboratory of Polskie Zakłady Lotnicze Sp. z o.o. The right-hand gear leg was attached to the rig as in the aircraft – see Fig.4. The wheel axle was loaded through the wheel bearings. The braking moment was applied to the wheel axle as a pair of forces, which can be seen in Fig.4. The applied loads were:

- vertical force,
- side force,
- fore and aft force,
- braking moment.

The following loads have been taken into account in the test program: loads resulting from taxiing on prepared and unprepared airfields, maneuvering (side force), braking and landing, as required by the MIL-A-8866C norm. The load spectrum (vertical loads) due to taxiing on an unprepared airfield was measured during the taxiing tests on the emergency strip of the Mielec airfield.



Fig. 4. The main landing gear on a stand during fatigue testing (front-side view). The test is performed in the structural tests laboratory of Polskie Zakłady Lotnicze Sp. z o.o.. The test program was adapted from that prepared by the Institute of Aviation in Warsaw for the previous main landing gear

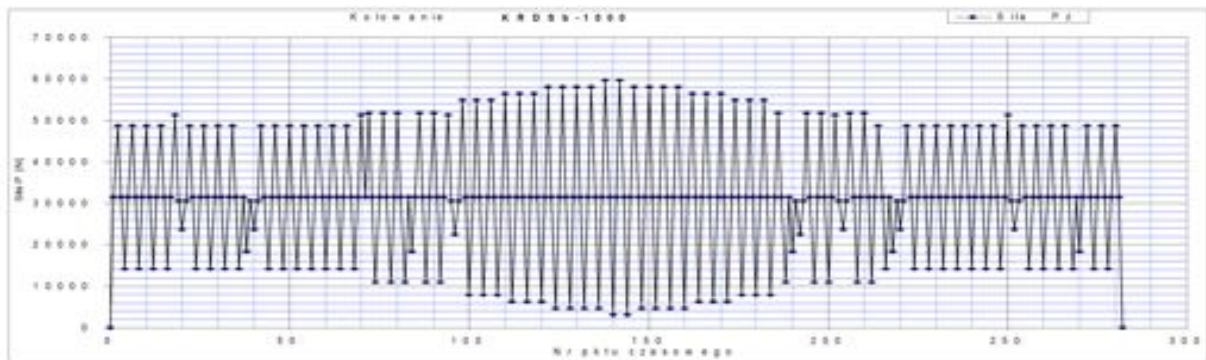


Fig. 5. A typical plot of vertical force during one flight in the new main gear fatigue test

The test was performed in a flight-by-flight manner. One flight contained about 50 cycles – see Fig. 5 for vertical force variation in a sample flight. Because there were 6 applied taxiing load levels and 10 landing load levels, there were 14 load combinations defining the particular flights. The full spectrum of flights was performed in 1000 flights.

The loading system was the MTS Aero 90-LT with four loading channels.

Twelve strain gauges were installed on the leg in order to monitor the structural integrity in the most heavily loaded places and to check the calculated stress levels. Initially, two sections of the leg were recognized as critical:

- section below the upper weld region with maximum calculated stress level of 498 MPa (section A-A in Fig.2),
- section above the lug for mounting the shock-absorber with maximum calculated stress level of 473 MPa (section B-B in Fig.2).

The shock absorber was omitted.

During the test a crack occurred in the shock-absorber cylinder – see Fig. 6. The FEM analysis of the damaged area showed a local stress concentration due to a small radius of the undercut at the end of the thread for mounting a nut – see Fig. 7.



Fig. 6. The new landing gear shock absorber with a visible crack at the bottom end of the cylinder

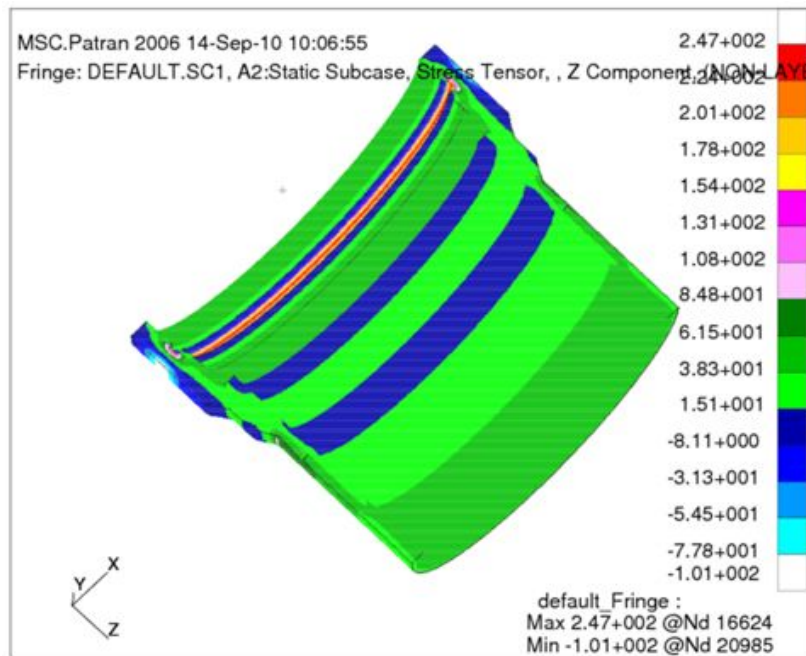


Fig. 7. A stress map of the loaded shock absorber cylinder inner surface as a FEM analysis result.

The cylinder is loaded by internal oil pressure and the force acting on the nut

It was determined to continue the test for the landing gear with a mock-up shock absorber, in order to gain time to develop and introduce design changes to the shock absorber. The modified shock absorber was tested at a separate rig – see Fig. 8. Only one loading channel

was required. The axial force spectrum from the Full Scale Fatigue Test was applied – see Fig. 9.



Fig. 8. The modified shock absorber on a stand during fatigue testing

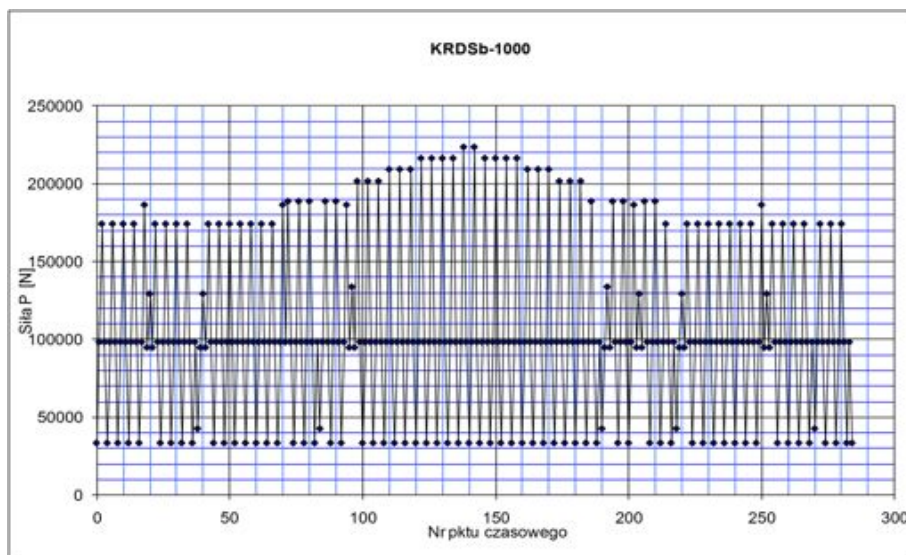


Fig. 9. The axial force spectrum applied in the shock absorber fatigue test

Ten strain gauges were installed on the cylinder in order to check the calculated stress levels and monitor the structural integrity at the most heavily loaded places.

During the Full Scale Fatigue Test of the new main landing gear and the fatigue test of the modified shock absorber, cracks in other parts were observed. However, it is relatively easy to replace these parts during airplane operation.

The test results for the leg have been satisfactory so far. The test of the modified shock absorber is going on and will be accomplished soon.

To sum up, the fatigue tests of the new main landing gear for PZL M28 aircraft showed significantly longer fatigue life compared with the previous structure (more than 3 times). It is worthy to emphasizing that:

- (1) the new landing gear is fully interchangeable with the previous structure, and the same wheel, brake and wheel axle were used;
- (2) the total main landing gear weight increase was below 6 percent.

(Research supervised by Józef Brzęczek, Polskie Zakłady Lotnicze Sp. z o.o., Mielec).

2.2 Airworthiness Tests of the UAV Structure - Fatigue Issues

A significant increase in the applications of UAVs has been observed in the last two decades – mostly in the military domain. At the same time the economical aspects have raised interest in the application of UAVs also for civilian purposes. The potential possibilities of such applications include: terrain monitoring during disasters, monitoring of forests and crops, monitoring of communication tracks, media or energy transfer lines etc. Undoubtedly, the use of UAVs would be cheaper than that of GA aircraft. The main obstacle here is the lack of law requirements concerning the use of air space by UAV aircraft. It is a challenge for the scientific community to make UAVs available for civilian purposes. Preliminary investigations related to strength and fatigue safety of the UAV structures were performed. Those investigations were carried out under the UAVs development program conducted at Warsaw University of Technology. The object of investigations was SAMONIT 1 – an UAV destined for from-air monitoring missions. The basic data of this aircraft are displayed in Fig.1.



Fig. 1. SAMONIT 1 and its technical data

SAMONIT can be controlled either in a manual way (by a RC device) or in an automatic way – by a MicroPilot L-2128 (Fig. 2). Attention was focused on the load spectrum induced by both ways of the UAV control. Knowledge about load spectrum is necessary to define fatigue durability requirements of the UAV-

structure to be included in the UAV airworthiness regulations.

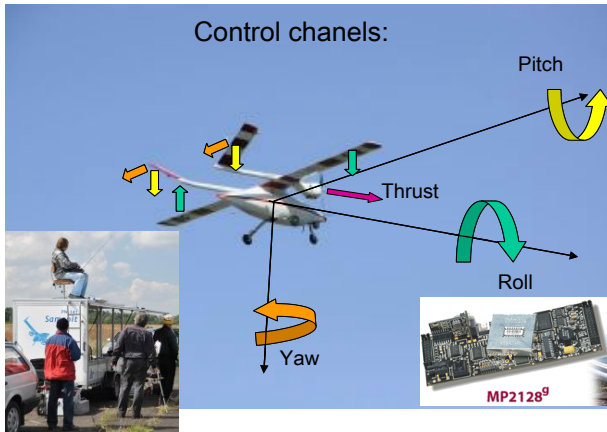


Fig. 2. SAMONIT 1 – control channels

Besides its main function of controlling the aircraft, the autopilot has another useful feature of acquiring flight data (the total of 52 channels). Those data are of great importance for flight dynamics analysis including load spectrum derivations.

Figure 3 shows a screen-shot of the MicroPilot software for data-log viewing.

The upper window contains some selected

signals: airspeed, altitude and acceleration in the z -axis direction (i.e. perpendicular to the wing-plane), while the lower window contains the GPS-track. The analysis focused on the a_z acceleration signal because it may be easily recalculated into the load factor n_z as a ratio of a_z/g , where g is Earth's gravity.

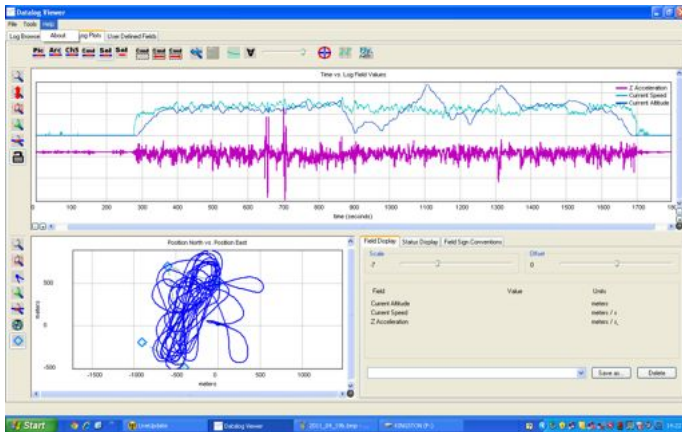


Fig. 3. Data-log Viewer – screen-shot of MicroPilot software

As a tool for load signal analysis there were used Transfer and Half-Cycles arrays. The transfer arrays (T-arrays) contain information regarding number of signal transfers from each particular level to another level. The signal range in MicroPilot data-log is divided into 128 levels, however, for

the purposes of the present investigations, the number of signal levels was reduced to 32 per range. Thanks to this simplification it was possible to apply the software tools previously used by the author in investigations of composite gliders' load spectra. There was also applied a standard correlation between n_z and load level LL , i.e. $LL=3$ for maximum design value of the n_z , and $LL=31$ for minimum design value of the n_z .

To be able to count signal transfers a load signal should be first reduced to the form of a local extremes chain. Subsequently, either the algorithm shown in Fig. 4 or the Rainflow counting algorithm shown in Fig. 5 should be applied. The result obtained in the second case is a specific transfer array called a half-cycle array (HC-array). The important feature of a T-array and HC-arrays is a so-called operational zone (Fig. 4), i.e. a square envelope of all cells having non-zero values. This envelope defines the range of signal variability and is marked on the T- and HC-arrays as a darker square. Operational zones of the T-array and HC-array derived from the same signal have equal dimensions, but only HC-arrays can be used in fatigue damage calculations because in a basic T-array does not register the resulting changes of signal levels after several transfers.

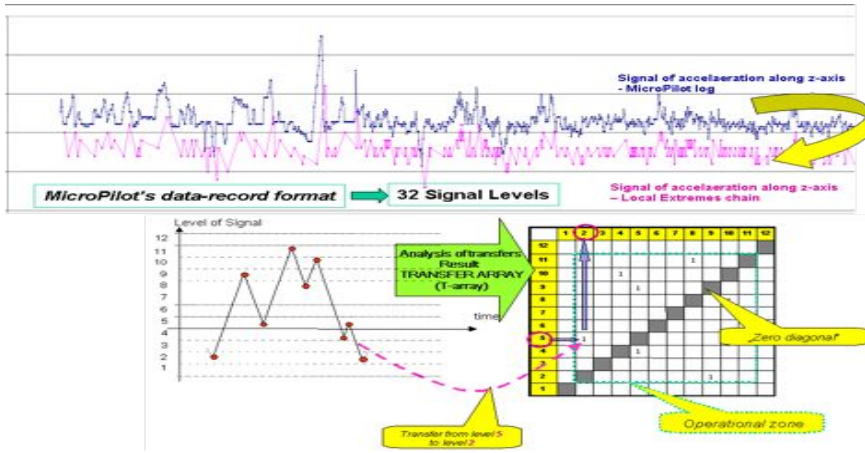


Fig. 4. Signal elaboration and Transfer-array determination

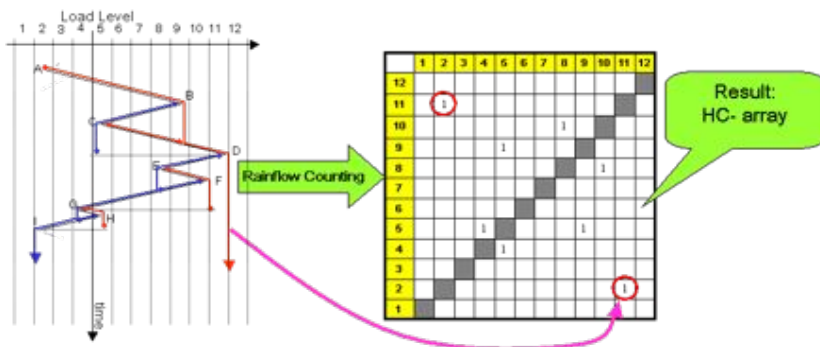


Fig. 5. Half-Cycle array as a result of applying Rainflow Counting algorithm

On the basis of the HC-arrays it is possible to create an incremental form of load spectra (Fig.6). A basic form of load spectrum presentation in the past, today an incremental form of load spectra has is of limited value for fatigue calculations, but still can be used for comparative analysis of different load spectra.

As an example there are shown incremental load spectra derived from the T-array and the HC-array obtained from the data-log. The flight considered was named Flight No.1 and is presented in Fig. 7. In this flight the UAV was controlled partly in an automatic and partly in a manual mode. The track length was about 41 km and the flight duration was about 950 s.

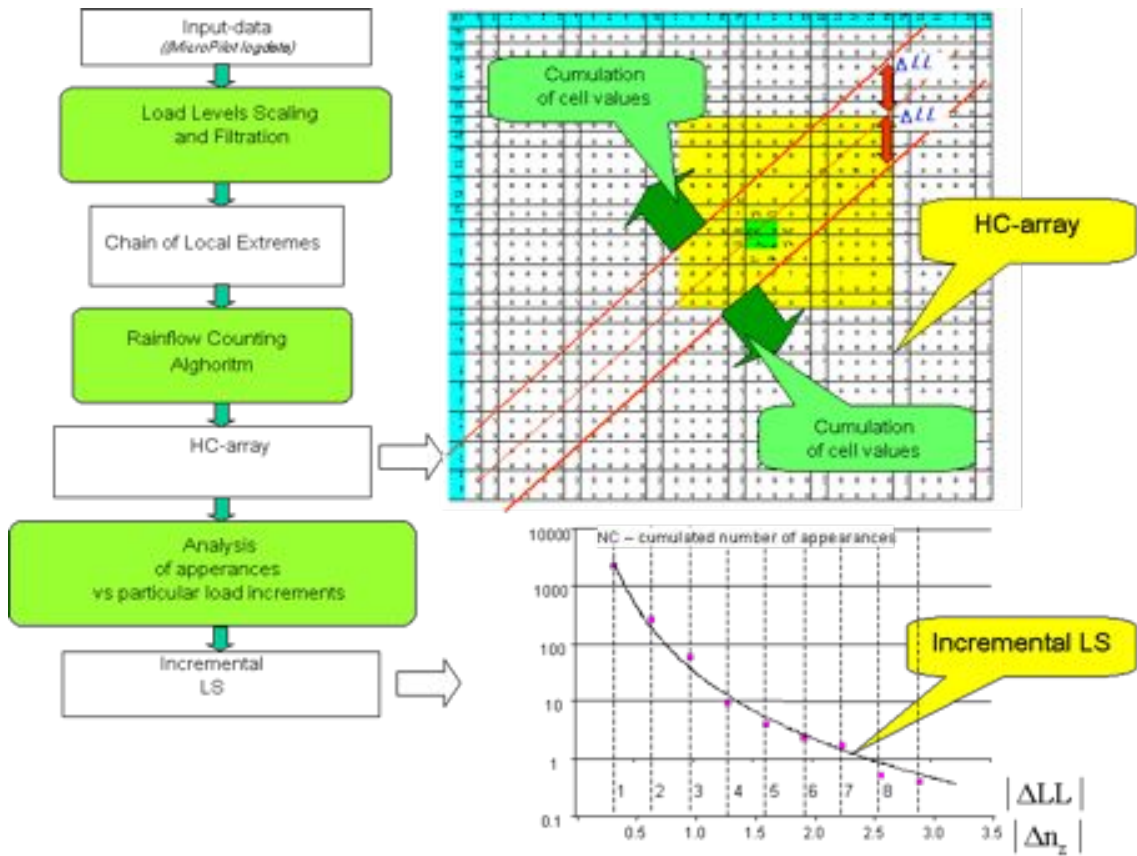


Fig. 6. The procedure of incremental load spectrum derivation

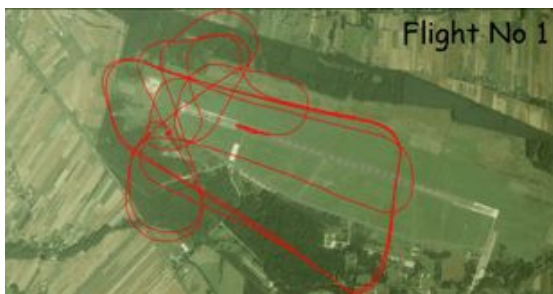


Fig. 7. Track of Flight No. 1

As it can be seen in Fig. 8, the maximum value of load increment is much lower in the case of applying the basic T-array algorithm that makes the reason why the Rainflow Algorithm is so important in fatigue calculations.

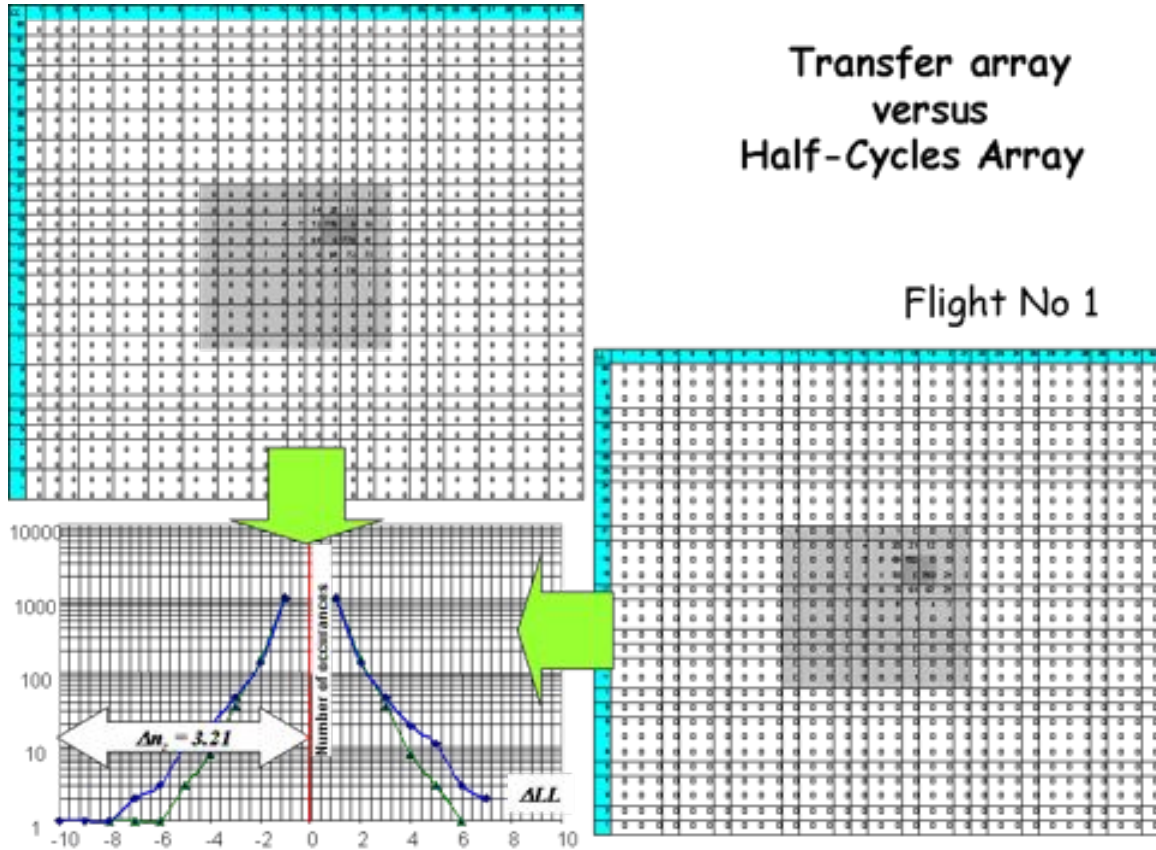
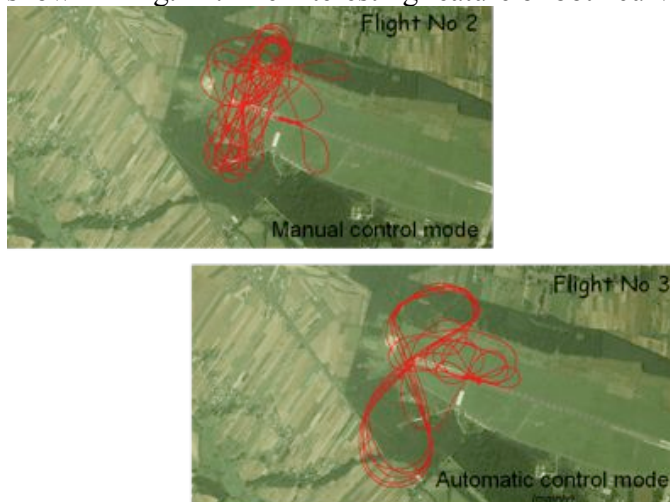


Fig. 8. T-array versus HC-array derived from the same signal

The presented tools were used for comparison of load spectra derived from the logs of two subsequent flights of SAMONIT 1: Flight No. 2 was made in a manual mode, while Flight No. 3 was mainly controlled by the autopilot. Both flights were made at the same airfield in similar weather conditions (Fig. 9). The times of flights were: 22 (Flight No. 2) and 17 minutes (Flight No. 3).

The HC-array from Flight No. 2 is shown in Fig. 10. The operational zone is larger here, and, interestingly, it contains the signal transfer between 10th and 27th LL (i.e. between $n_z = -1.71$ and $n_z = 3.75$). It is a significant variation, bearing in mind the fact that the UAV did not make any aerobatic evolutions.

In the case of Flight No. 3 – controlled by the autopilot – the operational zone was much smaller (see Fig. 11). Those observations are consistent with the incremental load spectra shown in Fig. 12. The interesting feature of both curves is a similarity in the range of $LL| < 7$.



The experiment leads to the conclusion that the autopilot mode produces a softer load spectrum than the manual mode of control does, but the number of flights being analyzed was too low to make any general conclusions.

Fig. 9. Tracks of flights No. 2 & No.3

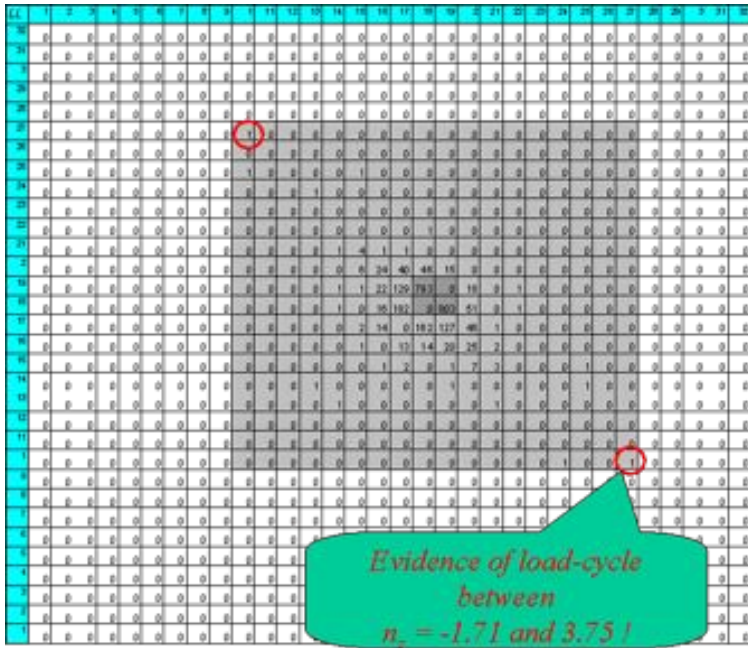


Fig. 10. HC-array from Flight No. 2 (manual control mode)

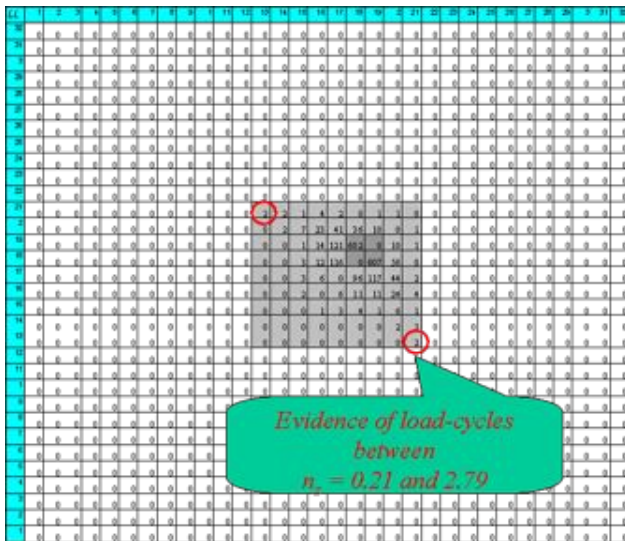


Fig. 11. HC-array from Flight No. 3 (autopilot control mode)

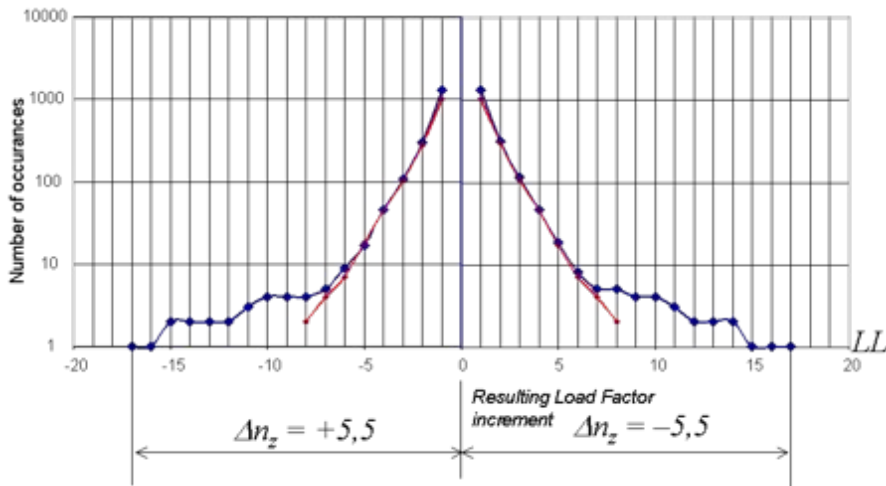


Fig. 12. Comparison of incremental load spectra generated by manual and autopilot control modes

Generally, to be able to determine effectively the UAV load spectrum it is necessary to increase the number of analyzed flights taking into consideration different scenarios, different weather and terrain conditions,, different pilots, etc. This would permit statistical analysis of occurrences of particular load increments. In the upper part of Fig. 13 there are two curves: the mean values and the values shifted up by 3 standard deviations. The latter curve takes into account possible dispersion of load increments occurrences (i.e. the number of appearances in relation to the flight times). On this basis it is possible to determine among other values the coefficients that should be applied for multiplication of the values existing in the **HC**-array compound from all analyzed flights in order to obtain more generalized results.

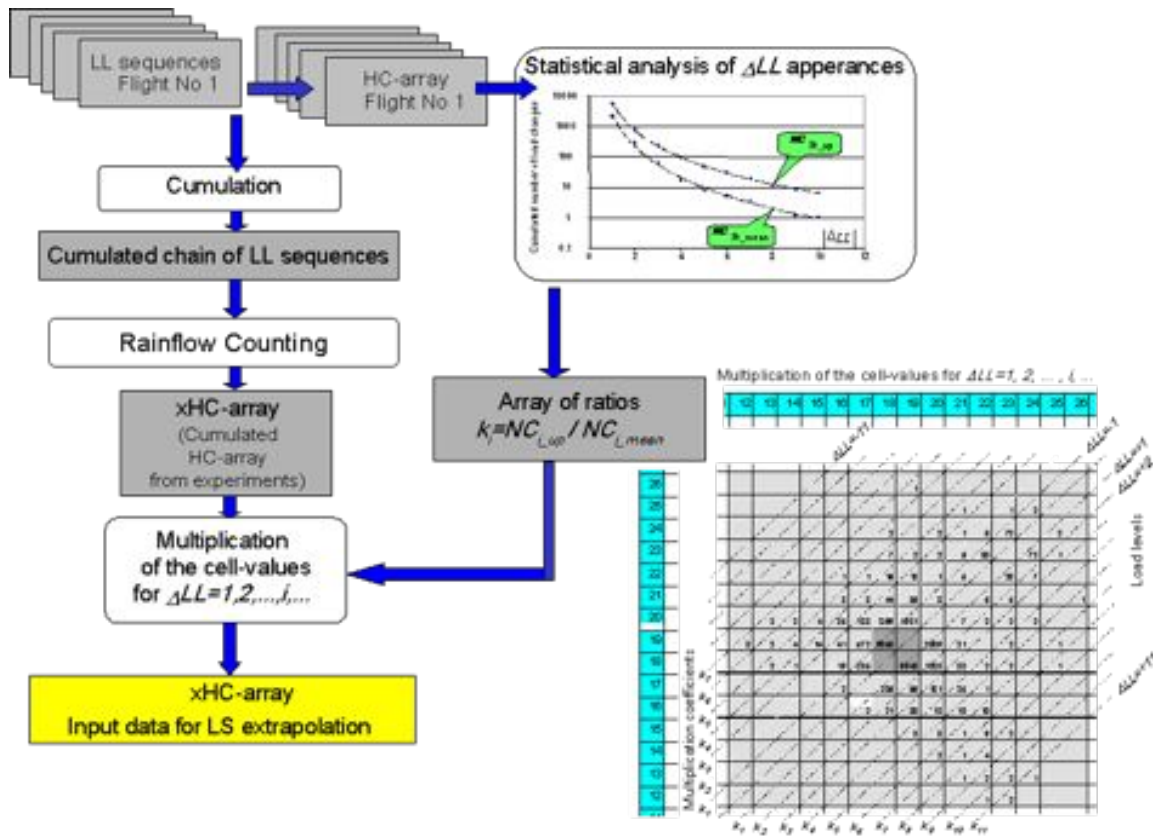


Fig. 13. Algorithm of data processing for model-load spectra – general case

Fatigue tests

This part describes selected strength or fatigue tests for which load spectrum is of crucial importance. The first test concerns the spar of the UAV-SAMONIT1's wing (Fig. 14) made from CFRP composites.



Fig. 14. CFRP-wing structure of SAMONIT1

The main part of the wing structure is a wing spar. It can be tested together with the

whole wing. For economic reasons, however, a simplified composite torsion tube is quite often used in testing instead of the real wing skins. An important aspect of fatigue investigations is frequent control of fatigue damage propagation by means of the NDT devices (Fig. 15).

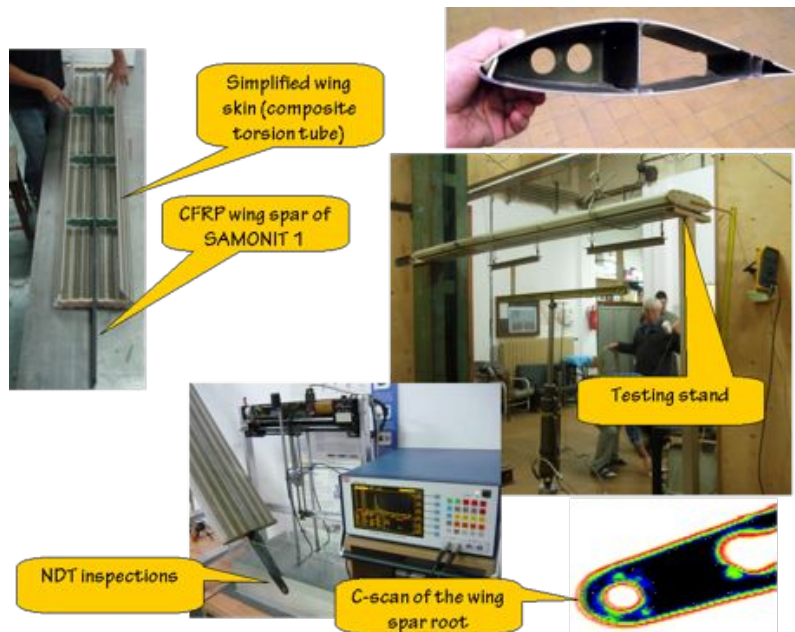


Fig. 15. Fatigue and NDT testing of SAMONIT 1's wing spar

Another element, which needs to be tested, is the tail beam, especially the joints between the beam and the aircraft structure (Fig. 16).



Fig. 16. Tail beam of SAMONIT 1

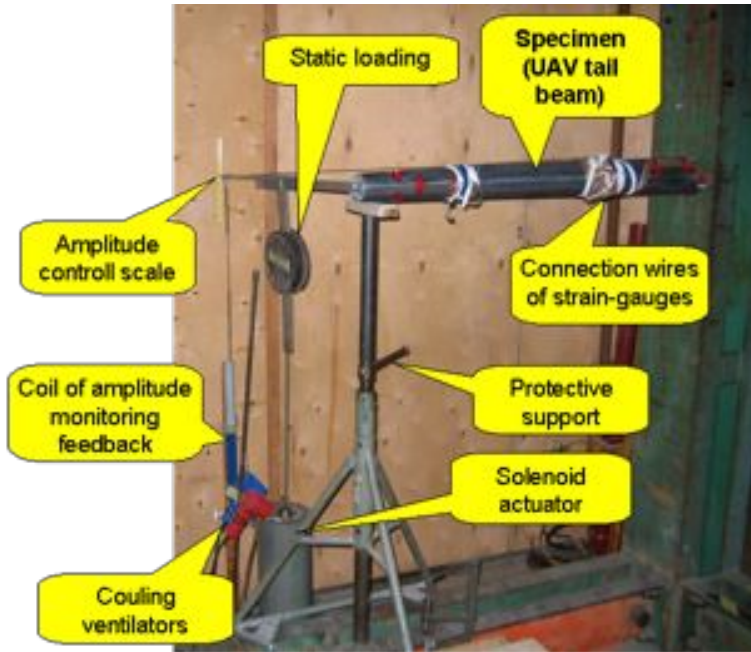


Fig. 17. Test-stand of UAV tail beam

Another crucial element of the UAV is the landing gear (Fig. 18). In comparison with GA aircraft this element is much more exposed to the damage risk because the UAV systems are not able to compensate for lack of the information normally accessible for the pilot seating in the cockpit.



Fig. 18. Landing gear of SAMONIT 1

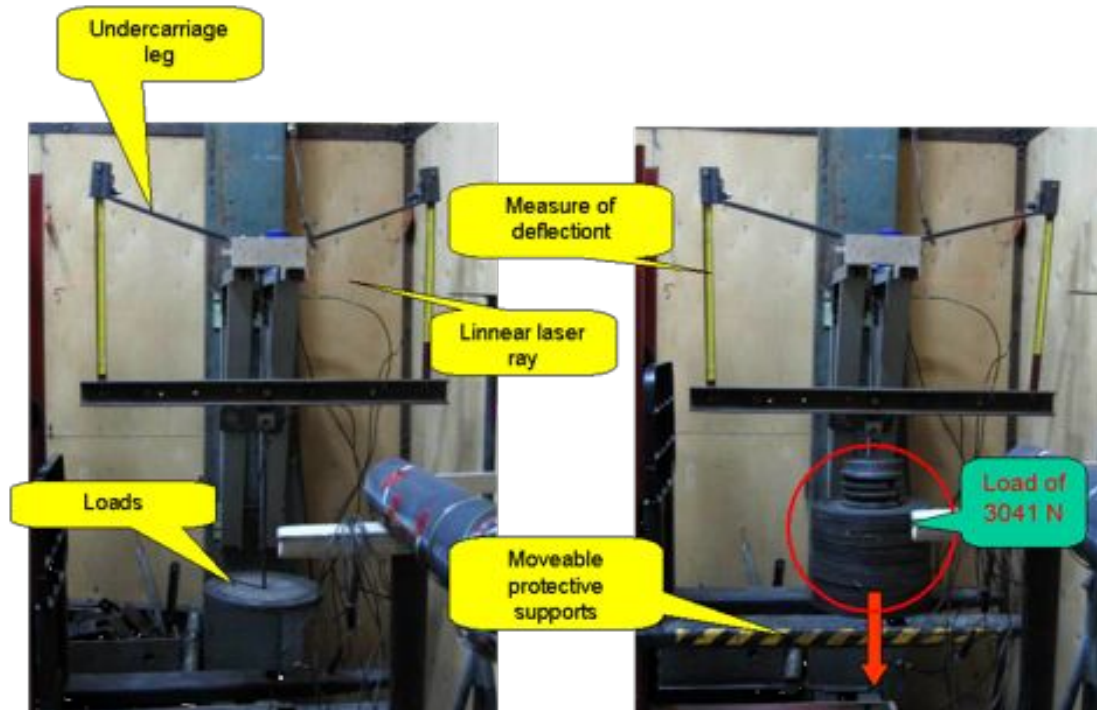


Fig. 19. Test-stand of UAV landing gear

To sum up:

- Determination of UAVs load spectra has a crucial importance for the process of elaborating airworthiness requirements for this category of aircraft.
- It was found that significant differences in load spectra could be observed between a manual and an automatic control mode of the UAV. Those differences may have strong influence on the fatigue life of the UAV structure.
- In order to determine airworthiness requirements for fatigue safety of the UAV structure it is necessary to increase the number of analyzed flights taking into consideration different flight scenarios, different weather and terrain conditions, different pilots, etc.
- Well-estimated load spectra and reliable fatigue tests are necessary to prove technical safety of UAVs.

(Research supervised by Mirosław Rodzewicz, Warsaw University of Technology, Warsaw).

2.3 Recent Progress in Full Scale Fatigue Test of Pzl-130 "Orlik" TC-II Structure

In 2009 the Polish Ministry of Defence contracted a modernization program for PZL-130 Orlik aircraft to convert it to the TC-II version. The modernization is accompanied by a research program to establish a new maintenance principle. The research program is called "SEWST" (*System Eksploatacji Według Stanu Technicznego*). The program consists of many different tasks but its main objectives concerning the service life assessment include flight tests, Full Scale Fatigue Test (FSFT), determination of Non Destructive Inspection technology routine and Teardown Inspection (TI).

The FSFT is currently being carried out at VZLU Praha in Czech Republic. The test article is a structure consisting of a retired fuselage after some modifications and a brand new wing, characteristic for the TC-II version, assembled by EADS PZL-Okęcie. The structure is loaded in a specially designed test rig by means of 20 actuators. Before the beginning of the test a calibration procedure was performed. Calibration results were compared and validated against the flight test results.

An intensive NDI program is planned to support the FSFT. There are three distinguishable levels of inspection accuracy. In the paper, brief information about the planned NDI activity is given including a description of each inspection level. The main deliverables of the project, the AFIT's work results and staff contribution to the project is highlighted in the following chapters.

Development of Load Spectrum

According to the SEWST program assumptions, the load block for the test was developed based on the flight loads measured during experimental flights, which were designed to represent the pilot training program for the PZL-130 airplane. This assured that the obtained loads were consistent with the mean flight profile for the PZL-130 "Orlik" TC-II in Polish Armed Forces (PAF). Measurements were carried out with an array of foil strain gauges described in.

According to the program assumptions the load block was to represent four main flight components: taxiing, flight, landing and buffeting. Flight and buffeting loads were developed directly using strain data gathered during flights. Since landings performed during the experimental flight program were, untypically, very smooth, the decision was made to develop landing loads separately according to the literature sources and the previously performed drop tests. Similarly, taxiing loads showed very low amplitudes and, due to limitations in the number of load lines within the load block, discussed in the following paragraph, couldn't be introduced directly. Instead, three types of artificial taxiing loads were developed: full stop, left and right turn; and were randomly placed within the load block. The level of loads was chosen based on the actual loads measured during experimental flights.

Time schedule of the FSFT and technical capabilities of the loading system imposed some limitations for the load block. Preliminary estimations showed that a ratio of about 120 load lines per flight hour (which gives 24 000 load lines in one block for planned 200 SFH) had to be achieved in order to finish the test on schedule. Since the sampling frequency of measured data was in the order of 100 Hz (400 Hz for buffeting loads), the amount of collected data was tremendous. In order to achieve the estimated ratio the gathered data had to be filtered.

The level of filtration was chosen using interactive methods. Based on the preliminary assumptions resulting from the flight profile defined by the Polish Armed Forces, representing 194 flights within the load block, flights were filtered and put together to achieve the number of lines close to the estimated. Since a further reduction was planned and it was necessary to increase the loading frequency for buffeting loads when only empennage actuators operate, the preliminary load block consisted of about 30 000 load lines.

The load block contained 194 flights with each flight involving the following components: taxiing, flight with or without buffeting, landing and final taxiing. The components were filtered and prepared separately and this is why it was necessary to verify load sequences after assembly in order to eliminate the load lines for which load levels for all 20 actuators differed by less than 5% or for which three subsequent loads for all actuators were either ascending or descending.

Since the test specimen was not fully constrained within the test rig it was necessary to assure that for all load lines the resultant forces would be in static balance. Additionally, loads acting on the structure were checked along with the N_z factor to make sure that the resultant mass of the aircraft was within a reasonable range (empty airplane and with fuel). After performing all the above steps, the final load block consisted of about 26 000 load lines, which was acceptable due to the possibility of the simulation of buffeting loads.

Introduction of Fatigue Markers

Since Teardown Inspection is planned after the completion of the fatigue testing it would be most beneficial to be able to determine the growth rate of expected cracks by means of Quantitative Fractography. There are several known techniques of introducing fatigue markers e.g. adding under/overloads or reordering loads within a load block. Since the main objective of the preparation of the load block was its correspondence to the actual PAF flight profile, introducing any artificial loads could change the block leading to false outcomes of the whole test.

The prepared load block, shown in Fig. 1a, exhibits local maxima due to significantly different severity of individual flights, which is consistent with the actual flight profile where aircraft is used both in training and display flying. Hence individual flights could be rearranged in such a manner that highly maneuverable flights were gathered in several groups of different lengths (Fig. 1b) resulting in distinguishable markers on the crack surface (Fig.2).

The influence of original and modified load blocks were tested using specially prepared Wedge Opening Load samples Fig. 3, manufactured from 2024-T3 aluminum alloy identical with the material used in PZL-130 "Orlik" TC-II.

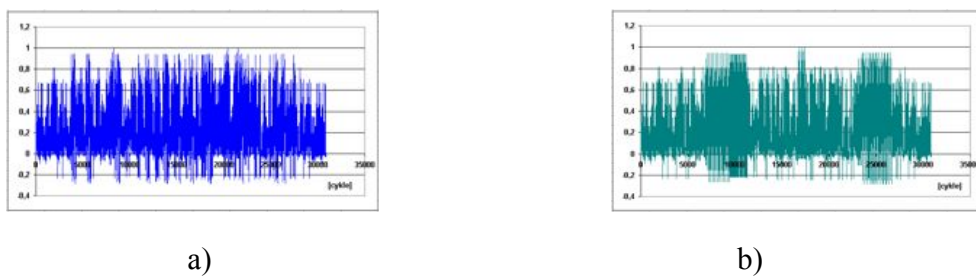


Fig. 1. Tested load blocks: a) before reordering, b) after reordering

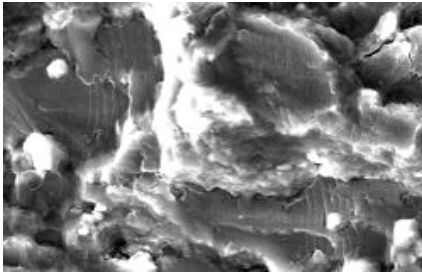


Fig. 2. Visible markers on the crack surface

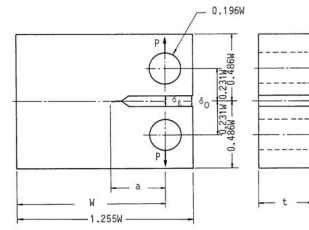


Fig. 3. Wedge Opening Load sample used in tests

Full Scale Fatigue Test Startup

The Full Scale Fatigue Test of PZL-130 "Orlik" TC-II is being conducted at Výzkumný a Zkušební Letecký Ústav. A PZL-130 "Orlik" TC-I aircraft was specially selected for the test purposes and modified according to bulletins to the TC-II version. The modernization consisted of overhauling the fuselage and assembling a new set of wings. The completed specimen consists of the fuselage, wings, landing gear and the engine mount. It was instrumented with the identical set of strain gauges as the specimen used previously by the AFIT during Operational Load Monitoring. The measuring system has two main objectives: validation of loads prepared for the purposes of fatigue testing and monitoring strain levels of crucial structural elements throughout the whole test.



Fig. 4. Strain gauges installed on the test specimen

Prior to the commencement of the test the strain gauge array was calibrated in a two-stage process. Firstly, loads used during the pre-flight calibration were used in order to verify the correlation between two installations. Secondly, actual load lines taken out from the prepared load block were tested in order to check the strain levels and stability of the specimen when extreme loads are applied.

Since the load block consists of over 24 000 lines that were directly calculated from flight loads, it was not possible to test all of them during calibration. Hence the first full load block was carried out at 30% of the total range in order to verify the stability of the specimen throughout the whole sequence.

After some minor modifications, e.g. caused by of some actuators reaching the end of the range, the setup was approved and the test was ready to start.



Fig. 5. Completion of loading system



Fig. 6. Test specimen mounted in test rig

Non-Destructive Investigation Program

During the whole test the structure will be monitored using various methods from simple visual inspection to eddy current or ultrasonic testing. According to the tripartite consultations between EADS, AFIT and VZLU the Non-Destructive Tests will be divided into three levels.

Level 1 is based on simple NDI techniques and will be carried out every 1000 ± 50 SFH. This inspection will be executed by VZLU in accordance with the NDI instructions delivered by AFIT. Estimated time for inspection is about 2 man-hours. No modifications to the test specimen or the test rig will be necessary.

Level 2 - inspection will require using advanced NDI equipment, so additional access to the structure will be needed. This level will necessitate a removal of clamps to grant access to aircraft structure. The inspection will be conducted every 5000 ± 1500 SFH for between 0 and 30000 SFH and the time interval will be shortened to $3000 \text{ SFH} \pm 1500 \text{ SFH}$ for $30000 \div 36000$ SFH. VZLU will also conduct this level of inspection in accordance with the NDI instructions delivered by the AFIT although first inspections will be conducted in presence of the AFIT qualified personnel. Estimated time for this inspection is 2 working days.

Level 3 - detailed NDI inspection including dismantling the wings and the fuselage. Four major inspections are planned throughout the test every $10\,000 \pm 2500$ SFH:

- $12\,000 \text{ SFH} \pm 2000 \text{ SFH}$;
- $20\,000 \text{ SFH} \pm 2000 \text{ SFH}$;
- $26\,000 \text{ SFH} \pm 2000 \text{ SFH}$;
- $33\,000 \text{ SFH} \pm 2000 \text{ SFH}$.

The AFIT will be responsible for this level of inspection. Estimated time for inspection is 5 working days.

A reporting routine valid for all levels of inspection has been developed. It includes detailed documentation of detected damage including photographic documentation and detailed definition of damage location as well as methods used to find and verify it. It will allow for a precise identification of damage and its location and enable tracking it throughout the test to verify its severity with relation to structural integrity. Reports will be developed by VZLU and delivered to the AFIT for interpretation and storage.

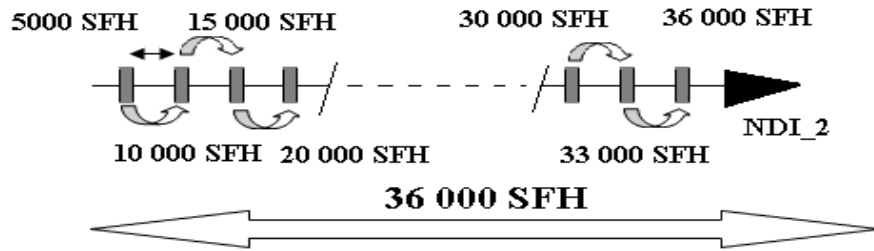


Fig. 7 General schedule of Non Destructive Inspections throughout the test

Troubleshooting and conclusions

In the preliminary stage of the test some minor problems occurred which were identified by alarming noises. In the first case there was a clear sound of the upper wing skin's buckling. After detailed examination it was decided that since this phenomenon appeared only for high levels of N_z the test will be carried out as planned but with special care taken during inspection of the wing's upper skin. The latter case was identified in the main landing gear region. In this case it appeared that the noise was caused by friction between the landing gear and the wing structure due to lack of grease between these two components. After supplying additional grease the alarming noise stopped.

The test is scheduled for 36 000 SFH. During the first three level 1 inspections, after 1000, 2000 and 3000 SFH, no damage in the structure was found. Conclusions from these investigations along with further conduct of the fatigue test will be presented.

(Research supervised by Andrzej Leski, Air Force Institute of Technology, Warsaw).

2.4 Preliminary Verification of Selected Solutions for Crack Detection

Currently, a big number of modern and innovative crack detection solutions are being developed. Unfortunately, there is lack of verified data from reliable, autonomous R&D centers, confirming efficiency of those approaches. For that reason, special preliminary laboratory studies were conducted to verify the two selected measurement systems.

Laboratory tests were performed to explore the reliability and sensitivity of the DMI SR2 optical system along with the resistive ladder sensors for crack detection. For this purpose appropriate specimens were prepared and examined under variable loads until a visible fatigue crack occurred.

Optical Strain Measurement using Polymer Gages

An initial verification of the DMI SR2 system was carried out. The system, which is an optical solution for determining deformation, also called direct strain measurement, is similar to the digital image correlation method. The captured images of a specified specimen area (in the unloaded and loaded state) are used to define the extent of deformation for a short line segment visible on the specimen's pattern.

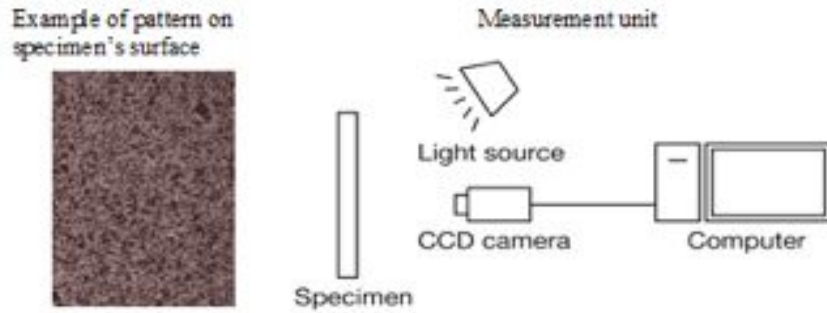


Fig. 1. Components of optical strain measurement system

The DMI SR2 system utilizes a very unique pattern, which consists of a polymer gage permanently bonded to the specimen's surface. There is a precise geometrical pattern on each of the gages, which is used to determine strain, and also for self-identification purpose within the rest of the system. The gage is fitted to the structure using the same method that is used for foil strain gages. The view of the gage is shown in Figure 2.

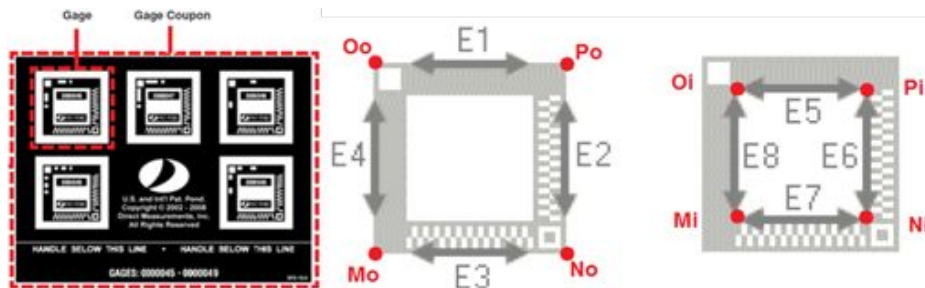


Fig. 2. Polymer gage coupon and characteristic edges

The polymer gage has 8 characteristic nodes (4 inner – Mi, Ni, Oi, Pi, and 4 outer – Mo, No, Oo, Po), which gives 8 independent measurement line components. Gage deformation is determined separately for each line element, using a sensor with a digital camera connected to a PC equipped with dedicated software. By comparing strain values at different edges of the sensor (on the parallel, opposing line segments) it is possible to detect cracks and determine the direction of crack propagation.

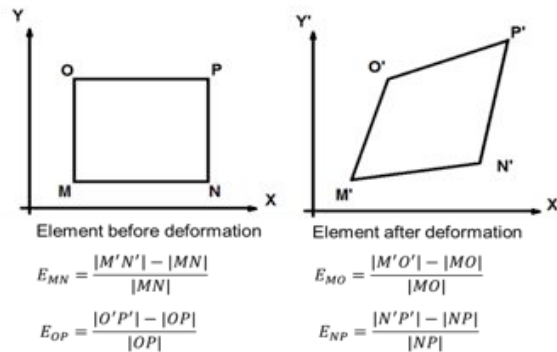


Fig. 3. Non-uniform strain with equations

The gage measures directly uniform (similarly to the 90° rosette foil strain gage) or non-uniform deformations. Non-uniform or differential deformation of the opposing sides of the gage indicates non-uniform plastic strain (fatigue) or a crack. The software algorithm calculates strain in μStr using equations in Figure 3.

The Conduct of Testing and Test Results

Preliminary tests were conducted on two types of specimens using a fatigue test system. The first one was a flat, rectangular specimen with a small, 3 mm fastener hole. The second specimen was a flat element with an "omega" type stiffener, interconnected with the rivet seam. Both specimens were made of PA7 aluminum, with dimensions H160xW50xT2 mm. The load was applied at a frequency of 10 Hz. Measurements were conducted under two load values for each polymer gage. The results were illustrated in the graphs, separately for the inner and outer components of the gage.

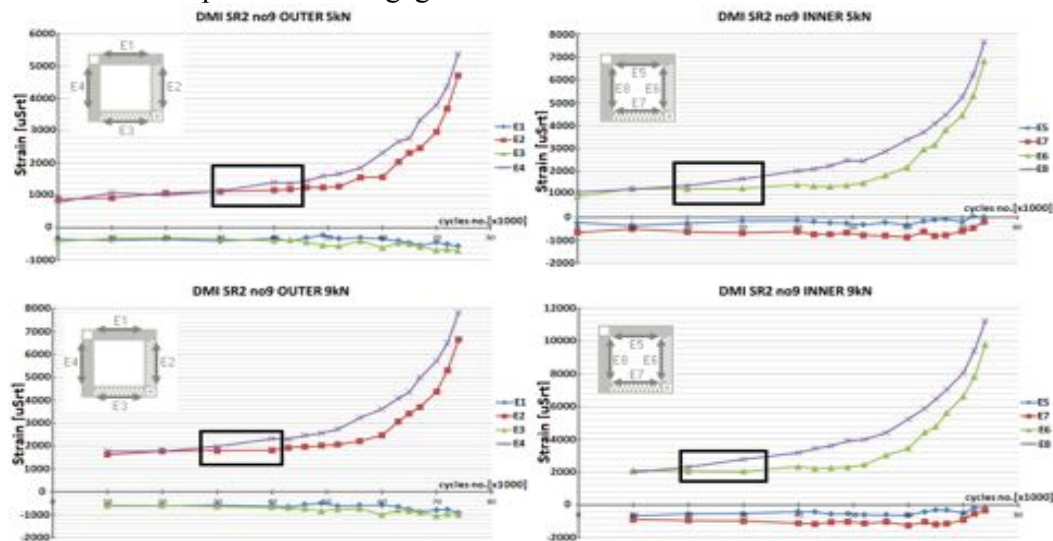


Fig. 4. Test results for a flat specimen with a fastener hole under 5 kN and 9 kN axial load

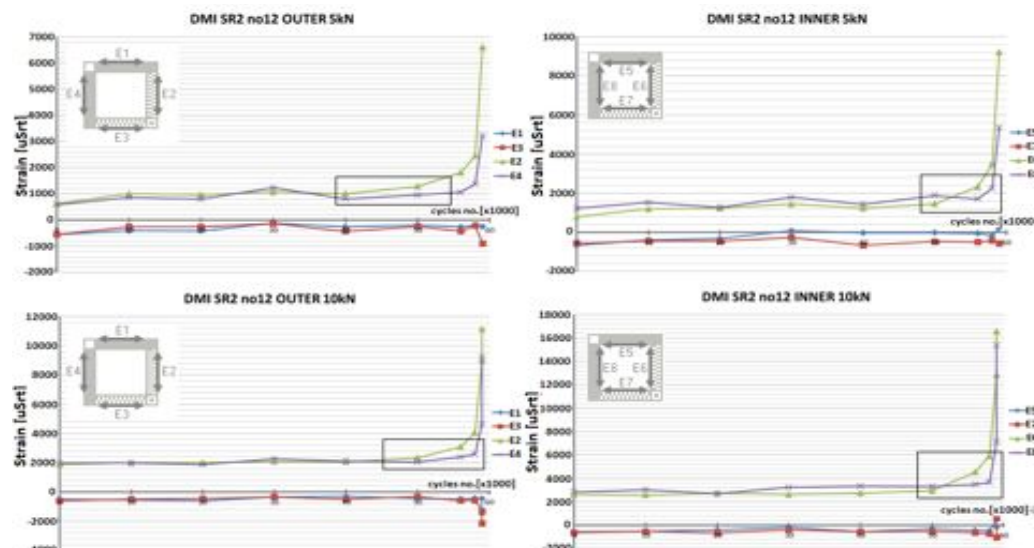


Fig. 5. Test results for a flat specimen with a riveted joint under 5 kN and 10 kN axial load

Test results are quite promising for both types of specimens. At the first stage of the test, strain values for opposing edges of the polymer gage are similar. Black rectangles in the charts mark the initial state in which the gages sense any anomalies around the fastener hole. A difference between strain values grows because of a crack developing only on one side of the hole. The inner edges of the gage respond faster than the outer ones due to a closer location to the hole. This fact confirms the possibility of detecting fatigue fractures in the

structure and determining their direction. On the other hand, accuracy and stability of data increase as the load applied to the specimen grows.

Crack Detection using Resistive Ladder Sensor

Preliminary studies of electrical resistive ladder sensors were also conducted. The sensor's structure is similar to that of foil strain gauges. Differences in shape of the measuring grid, designed as a parallel connection of thin conductive paths, can be noticed. The method of integrating the sensor with the structure is identical to the one used for foil strain gauges.

When a crack opens under the sensor, a local deformation occurs and the foil with the paths is gradually torn apart. This progressively stops electric conduction. The signal from the sensor changes in accordance to Ohm's Law. This way, by fitting such a sensitive element in a location suspected of surface cracks and measuring its resistance, the possibility to detect and quantify fatigue fracture arises. In the investigation, two sensor types were compared.

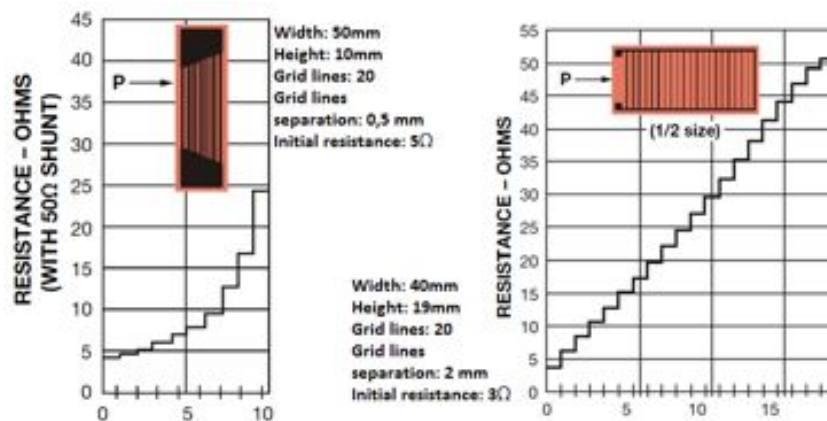


Fig. 6. Resistance characteristics of two types of resistive ladder sensor

To be able to perform measurements with the resistive ladder sensors, it was essential to develop a special electronic circuit. As a data recorder, an appropriate 16-bit A/D converter card was used, connected to a PC computer.

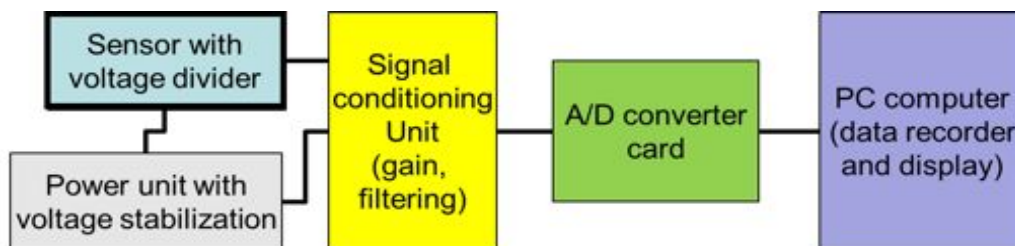


Fig. 7. Resistive ladder sensor measurement system components

The Conduct of Testing and Test Results

Preliminary tests were conducted on flat rectangular specimens with little notches on one edge using a fatigue test system. Specimens were made of PA7 aluminum, with dimensions H160xW50xT2 mm. The applied axial load was in the range of 7-12 kN, at the frequency of 10 Hz. The results were depicted in the graphs, separately for both types of ladder sensors (A and B), for two test runs.

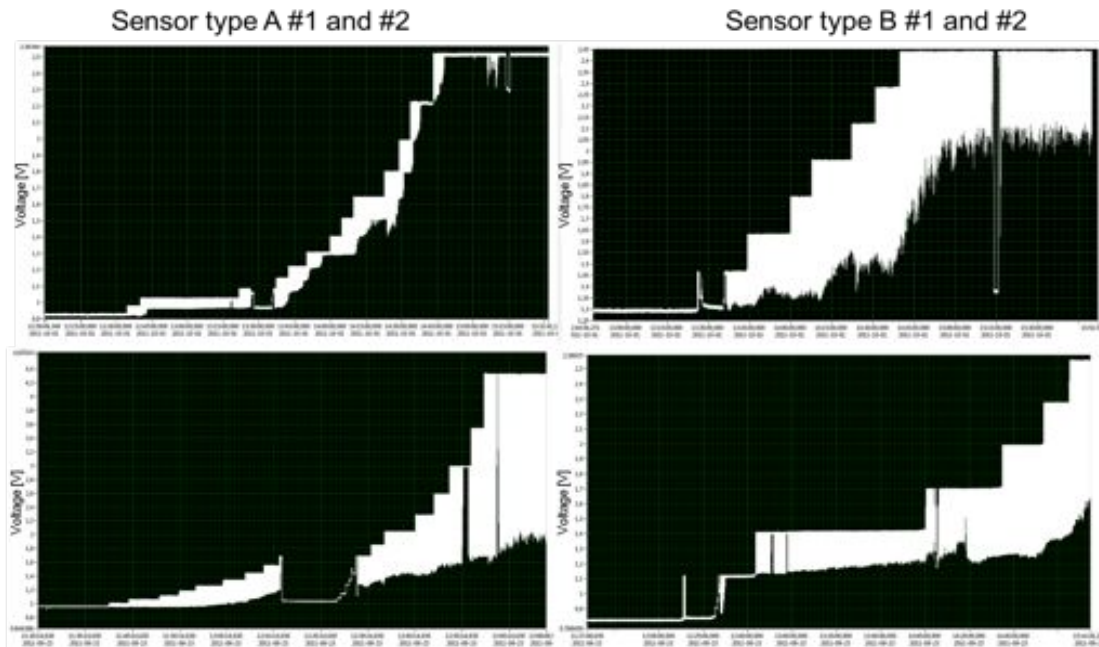


Fig. 8. Test results for type A and type B ladder sensor for two identical specimens

Test results confirmed that it is possible to detect and quantify fatigue cracks with both types of ladder sensors. Some modifications in the signal conditioning unit are required, especially in gain and filtering, to increase voltage resolution and range, as well as to purify measurements from unwanted peaks and valleys. Stability and sensitivity of the sensor was satisfactory and the method is suitable for real-time measurements.

Conclusions

In this work, preliminary verification of two crack detection methods was performed. Both methods are capable of detecting fatigue cracks in the structure, although their principles of operation differ substantially. Further experiments are essential to confirm repeatability, reliability and accuracy of measurements on more complex structure areas.

Along with the collected data, the present preliminary verification study provided some practical knowledge not only about potential future applications and types of measuring approaches (*in-situ* or real time), but also about labor intensity of data post-processing as well as the field of fracture detection. Table 1 summarizes these observations and compares the two presented crack detection solutions.

TABLE 1. Comparison of presented crack detection solutions

Optical polymer gage solution		Resistive ladder solution
1.	permanently integrated with the structure	permanently integrated with the structure
2.	no wires, no power supply to the sensor	needs additional wires for data and power
3.	no additional measurement circuit	needs signal conditioning and A/D converter
4.	operator is needed for measurements	no operator is needed for measurements
5.	access to a gage is essential	access only during installation
6.	<i>in-situ</i> , off-line measurements	real-time, on-line measurements
7.	need for baseline measure	no need for baseline measure
8.	detects cracks and fatigue plastic strain	detects crack and quantifies its length
9.	detection in the area near to the sensor	detection of cracks under sensor
10.	labour-consuming post-processing	easy post-processing
11.	Accuracy depends on the operator's experience	accuracy depends on excitation voltage stability and electronic circuit quality

(Research supervised by Artur Kurnyta, Air Force Institute of Technology, Warsaw).

2.5 Introduction of Fatigue Markers in Full Scale Fatigue Test of an Aircraft Structure

Air Force Institute of Technology participates in the service life assessment programme SEWST. The aim of this programme, funded by the Polish Ministry of Defense, is to modify the operation system of PZL-130 "Orlik" TC-II turbo propelled trainer aircraft. The structural part of the programme is focused on the Full Scale Fatigue Test of the whole airframe.

At the end of the Full Scale Fatigue Test a teardown inspection is planned during which it would be most beneficial to be able to determine crack propagation rate by means of a crack surface inspection. Markers are usually visible on most fatigue crack surfaces, however they occur randomly therefore it is almost impossible to conclude anything about the crack history.

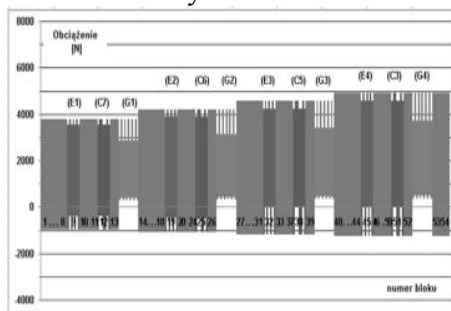
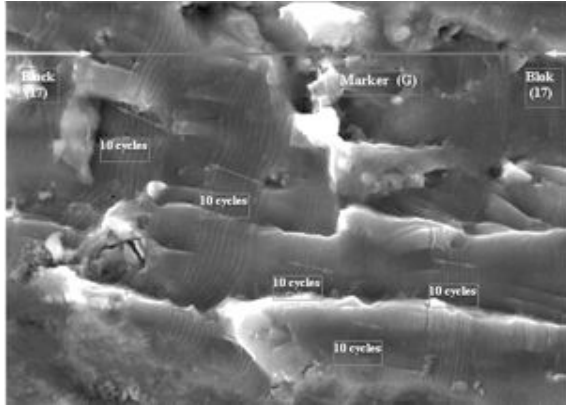


Fig. 1. A variant of load spectra for use during fatigue tests

Since the preliminary load block consisted of separate flights (flight loads together with landing and taxing loads) showing significantly different levels of severity, the easiest way to modify the load block was to change the order of flights within the block. Hence a pilot programme was started at the AFIT which was focused on the determination of the influence of flight sequence on crack appearance. Several load blocks were determined using various techniques of rearranging the order of flights within the preliminary load spectrum.

Since the overall intensity of the applied load spectrum and the consistency with the measured actual flight profile are crucial, the most favorable method of introducing fatigue markers is reordering flights within a load spectrum so that flights exhibiting the highest structural loads are cumulated in one or more groups, preferably of unequal length, in order to differentiate them during inspection, which will allow researchers to distinguish markers on the fatigue crack surface and analyze fatigue behavior of the tested structure and material.



This approach ensured the preservation of the initial severity of the load block and simultaneously enabled a significant increase in the probability of the markers occurrence introducing neither artificial underloads nor overloads that would most probably affect the crack propagation rate.

Fig. 2. Markers visible on the crack surface

Fatigue crack surfaces were inspected using Scanning Electron Microscope. As a result of the investigations a series of images were obtained showing the specimen microstructure with visible markers arranged in the desired sequences. Based on the obtained pictures the most promising load block arrangements were chosen for the Full Scale Fatigue Test.

(Research supervised by Andrzej Leski, Air Force Institute of Technology, Warsaw).

2.6 Numerical Simulation of Fatigue Fracture of the Turbine Disc

The work was focused on the crack propagation analysis of an aircraft engine turbine disc. In the first part of the work the finite element method was used for calculation of the stress state and the stress intensity factor (SIF, K_I , K-factor) in the turbine disc with an embedded quarter-elliptical corner crack, subjected to low-cycle thermo-mechanical fatigue. To refine the K-factor calculation, specially degenerated finite elements were used. These elements provide stress singularity suitable for the linear-elastic material of the disc. The performed calculations yielded the stress intensity factor K_I for different crack sizes. Subsequently, ΔK parameter was determined as a difference of the K_I values calculated for the turbine's speeds equal to 6373 and 14200 RPM. Based on the Paris-Erdogan equation and the obtained ΔK values, the fatigue crack growth plot for the turbine disc subjected to complex thermo-mechanical loads was determined.

In the first part of the work, a detailed geometrical model of the 1/89 turbine segment was created. The border surfaces of the disc used during the parametric 3D model definition are presented in Fig. 1a. The cyclic symmetry option with the appropriate boundary conditions enabled modeling only a small part of the disc with one blade.

The finite element program MSC-Patran was used to create both the geometry and discrete models of the disc segment and the blade. The finite element model of turbine presented in Fig 1b consists of about 23 608 solid elements. To model the mechanical interface of the adjacent surfaces of the disc and the blade, the "master-slave" type of contact with the friction coefficient of 0.1 was defined.

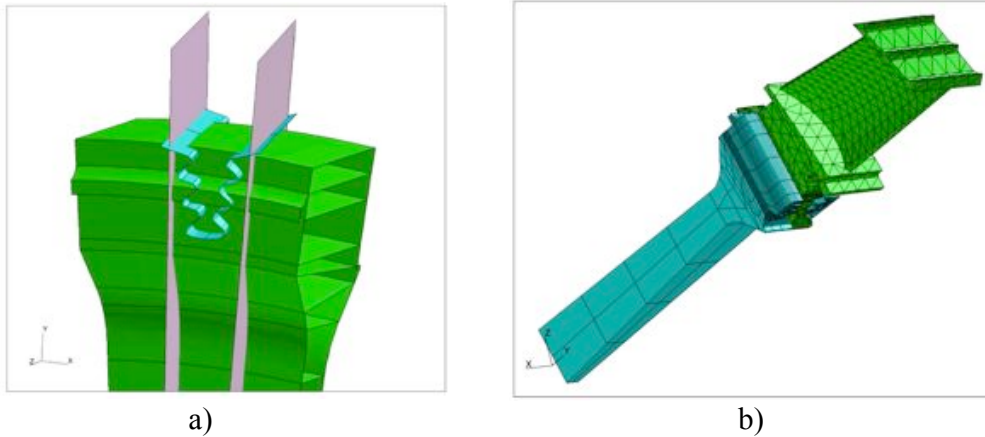


Fig. 1. Border surfaces used to create of the geometrical model of the disc (a) and the discrete model of the turbine segment used in computations (b)

A rotating hot section component in a turbine engine is in general subjected to a combination of surface (aerodynamic), centrifugal and thermal loads. Surface loads are associated with aerodynamic forces resulting mainly from the impingement of hot gases on the blade surfaces. The centrifugal loads arising from the mass of the rotated disc and the blades are usually the critical loads acting on the turbine disc. This load was determined through finite element calculation after defining the axis of symmetry, the rotational rotor speed and also the disc and the blade material density. In this analysis, the operational turbine speed of 14 200 RPM (rotation per minute) was applied. While the engine works, a non-uniform temperature field arises in the turbine disc and the blade. The thermal load used in the computations is presented in Fig. 2a.

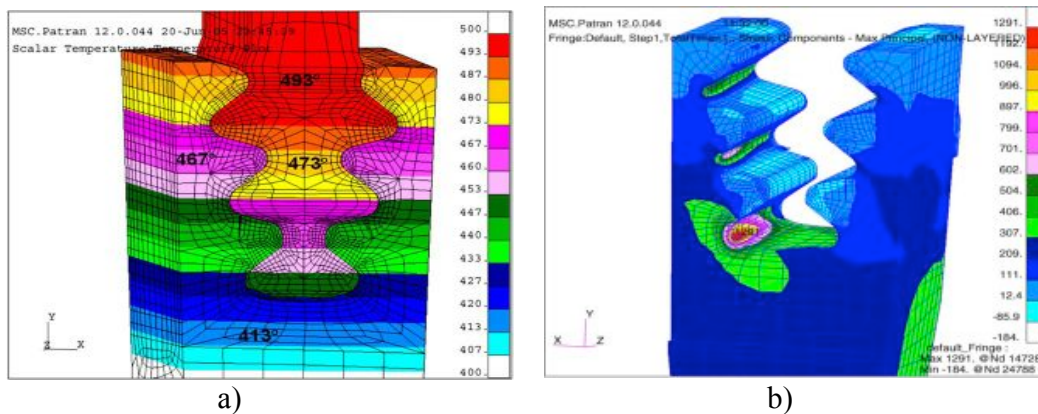


Fig. 2. The thermal field defined for the models of the disc and the blade in the dovetail-rim region (Celsius scale) (a) and the maximum principal (σ_1) stress distribution in the turbine disc subjected to thermo-mechanical loads (b)

Fig. 2b shows that the area of the maximum principal stress (1291 MPa) is located on the corner of the 3rd lower slot of the disc. The maximum principal stress is particularly interesting from the point of view of fatigue strength because it is tensile stresses that contribute the most to the fatigue fracture.

To refine the K-factor calculation (according to linear-elastic fracture mechanics), specially degenerated finite elements were used (Fig. 3).

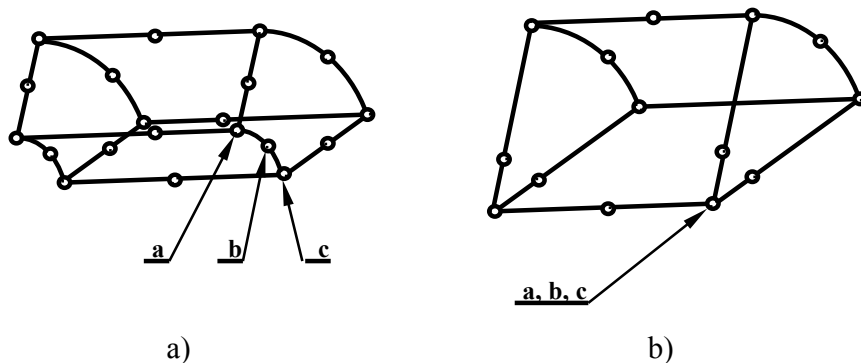


Fig. 3. Typical (a) and degenerated HEX-20 finite element

As a result of FEM calculations the stress fields for the disc with cracks were obtained. As a result of nonlinear computations, the stress intensity factor (K_I) for the quarter elliptical cracks was obtained. Based on ΔK values computed using FEM and the Paris-Erdogan solution, the crack growth curves were obtained for the disc with the rotation speed oscillating between 6373 – 14200 RPM.

The estimation of the K-factor and crack growth in the turbine disc subjected to thermo-mechanical fatigue is an original research work from the point of view of fracture mechanics and fundamental sciences in general. The results of similar analyses are not widely described in literature because of the complexity of the problem. Information about crack growth has great practical significance and can be useful to determine the periods between technical inspections of the engine. During these inspections, crack should be detected before its growth to the critical size. This kind of operation, known in literature as “damage tolerance” is used for the aircraft and turbine engines. The procedure (damage tolerance) can be used not only in aviation but also in many other branches, for different parts working in variable loads conditions.

(Research supervised by Lucjan Witek, Rzeszow University of Technology, Rzeszow).

3. NON-DESTRUCTIVE TESTS AND STRUCTURAL HEALTH MONITORING

3.1 Damage Detection and Size Quantification of FML with the Use of NDE

Introduction

Composite materials are now widely applied in aerospace structures. A new generation of structural composite materials for advanced aircraft is Fibre Metal Laminates (FML). The often used metal for FML is aluminum, and the fibers are glass, Kevlar or carbon. FML with glass fibers is called **GLARE** (**GL**ass **AL**uminum **RE**inforced), with Kevlar fibers is called **ARALL** (**AR**amid-fibre-reinforced- polymer/**AL**uminum **L**aminates) and with carbon fibers is called **CARAL** (**CA**rbon **RE**inforced **AL**uminum **L**aminates). Composite FML have been selected for application in aircraft structures because they have both low weight and good mechanical properties (high damage tolerance: fatigue and impact characteristics, corrosion and fire resistance). FML composites can be either in the form of laminar structures or sandwich structures.

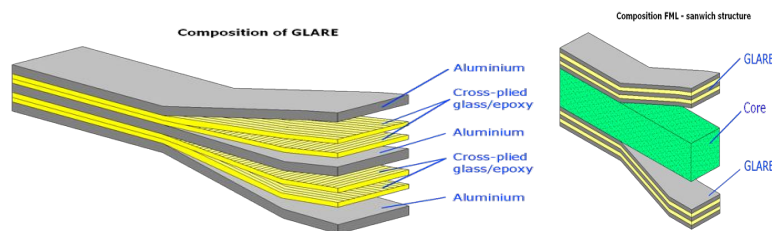


Fig. 1. Types of FML structures

An FML layered structure is particularly susceptible to the detachment of the layers. Also, delamination and cracks in the aluminum layers may occur as a result of stress.

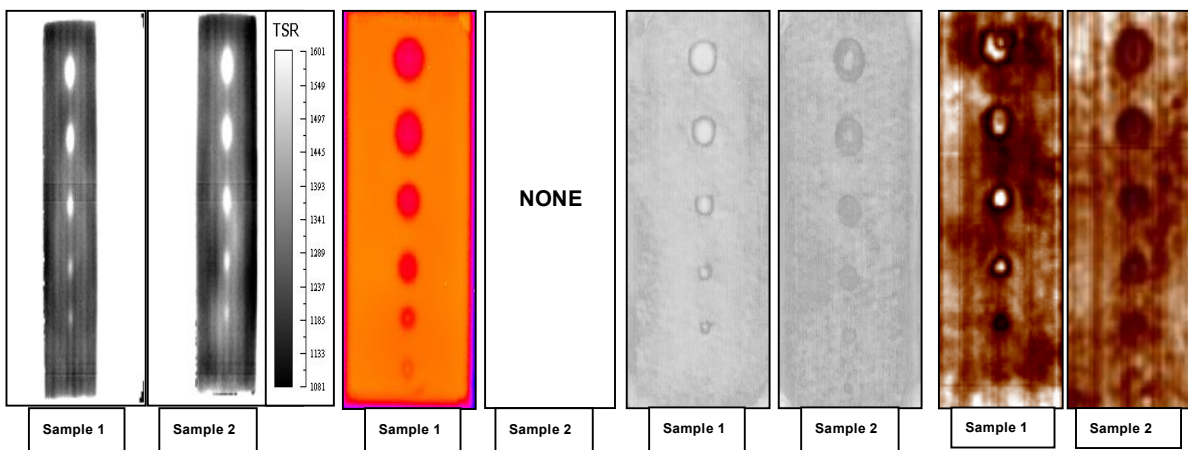
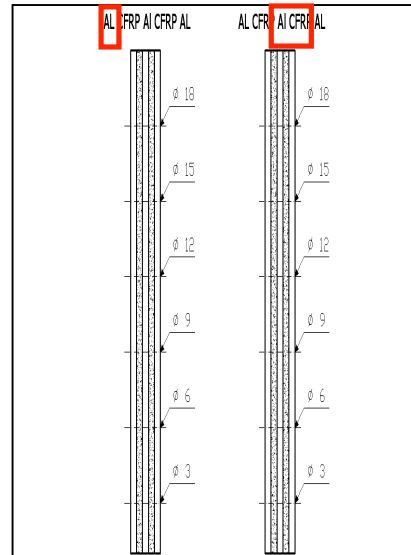
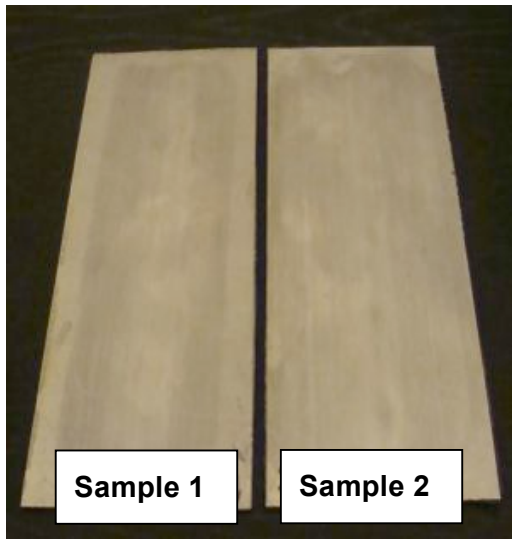
Quality control of materials and structures in aircraft is an important issue, also for FML laminates. For FML parts, a 100% non-destructive internal quality inspection during the manufacturing process is required. In the case of FML composites, the most relevant defects that should be detected by non-destructive testing are porosity and delamination as well as cracks in the aluminum layer.

For the purpose of monitoring the integrity of an FML structure, a combination of multiple NDT methods is commonly used:

- Visual (especially for inspections of fasteners and curved panels e.g. C & D checks of aircraft);
- Eddy Current (this technique is the best for crack detection in paramagnetic materials such as aluminum alloy);
- Ultrasonic (capable of detecting the following types of damage: disbonds, delamination, foreign object inclusions and impact damage);
- Thermography (capable of detecting the following damages: disbonds, delamination, foreign object inclusions and impact damage).

Results and Discussion

The non-destructive FML testing was made for the GLARE structures. For the sample no.1 in the aluminum layer and for the sample no. 2 in the laminate layer, the circle shape defects of different diameters were made. Fig. 2 shows the results of the C-scan inspection of a single Ultrasonic sensor, Phased Array, Eddy Current and Pulsed Thermography.



Pulsed Thermography

Eddy Current

Single sensor UT

Phased Array UT

Fig. 2. NDT results of Fibre Metal Laminate inspection

Analysis of the results enabled to determine the detection of defects by various NDT methods and to determine the accuracy of these methods. Fig. 3 shows defect size estimation determined by various NDT methods for the prepared specimens.

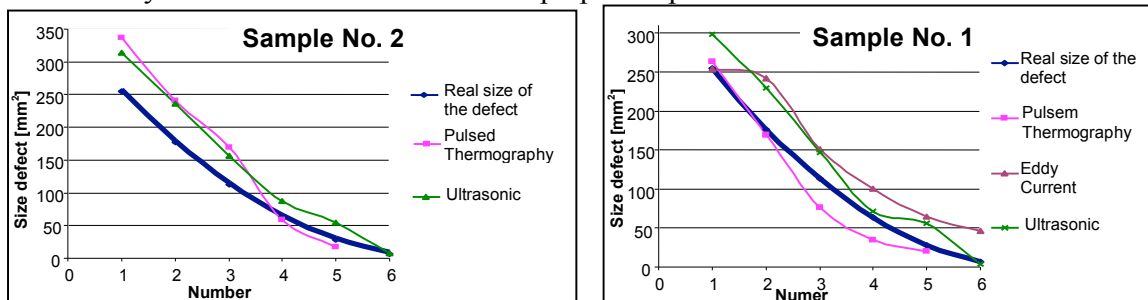


Fig. 3. Defect sizes determined by various NDT methods

The discrepancy between the size of the defect made in the specimen before the inspection and the size detected by the inspection with use of the ultrasonic method is due to the transmitter diameter and the beam divergence as well as the level of setting the threshold gates.

The sizes obtained using the eddy current method are also different from the actual sizes because of the so-called “edge effect” characteristic for this method.

Pulsed thermography method gave results in size estimation similar to the designed but it was not possible to detect all existing defects.

The samples were examined by the ultrasound method and then evaluated independently by five experts. The results were used to determine the PoD curve (Fig. 4).

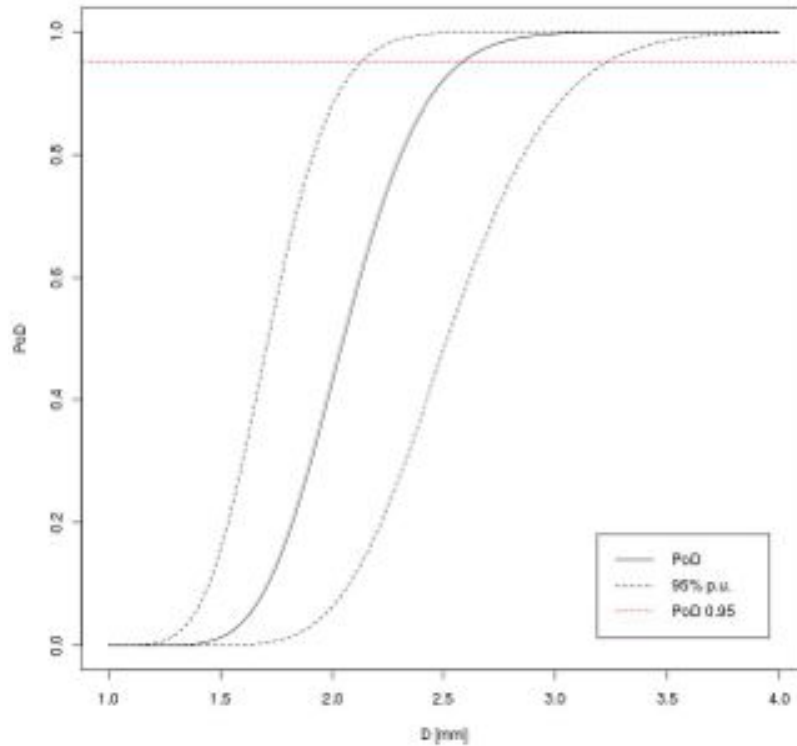


Fig. 4. PoD curve for ultrasonic method

Where:

D – diameter of the damage;

PoD – Probability of Damage Detection;

95% p.u. confidence interval for PoD curve;

PoD 0.95 - 95% level of the damage detection.

In the first step, the linear regression model was tailored:

$$\log \hat{a}_i = \alpha \log a_i + \beta + \varepsilon_i, \quad (1)$$

where \hat{a}_i equals the estimated size of the damage, a_i the real size of the damage, ε_i random measurement error. The use of least square method yielded the following model parameters estimators:

$$\alpha = 1.095 \pm 0.033, \quad \beta = -0.16 \pm 0.14. \quad (2)$$

The probability of the delamination detection of the damage size of the determined D size is given in the equation:

$$PoD(a) = P(\hat{a} > T) = \phi \left(\frac{\log T - \alpha \log \pi \left(\frac{D}{2}\right)^2 - \beta}{\sigma} \right), \quad (3)$$

where T is the selected threshold level, σ standard deviation of the measurement error ε , ϕ cumulative function of the standard normal distribution. Based on the confidence intervals or the parameters α, β it is possible to determine the 95% confidence interval for the given above $PoD(a)$ value. Moreover, the value $a_{0.95}$, for which $PoD(a_{0.95}) = 0.95$, was given based on:

$$\log(a_{0.95}) = \frac{\log T - \beta}{\alpha} + \frac{\sigma}{\alpha} u_{0.05}, \quad (4)$$

where $u_{0.05}$ means 95% quintile of the standard normal distribution. Estimated diameter size of the damage with 95% detectability equals:

$$D_{0.95} = 2.58 \text{ mm.}$$

Summary

The work highlights the inspection issues for the diagnostics of FML structures with the non-destruction methods based on the GLARE specimens. The use of NDT methods (ultrasonic, eddy current, thermography) gives the possibility to detect damage in FML composites. Ultrasound and pulsed thermography methods allow for the detection of defects in the entire volume of the material (detecting defects in the layers of aluminum and glass fibers).

Eddy current method can only be used to detect defects in the aluminum layers. The results of ultrasonic testing were used to create the PoD curve, which estimates the detection of defects possibility in FML for a 95% confidence interval. This approach enables to determine the accuracy of NDT methods.

(Research supervised by Krzysztof Dragan, Air Force Institute of Technology, Warsaw).

3.2 The MMM Expert System: From a Reference Signal to the Method Validation

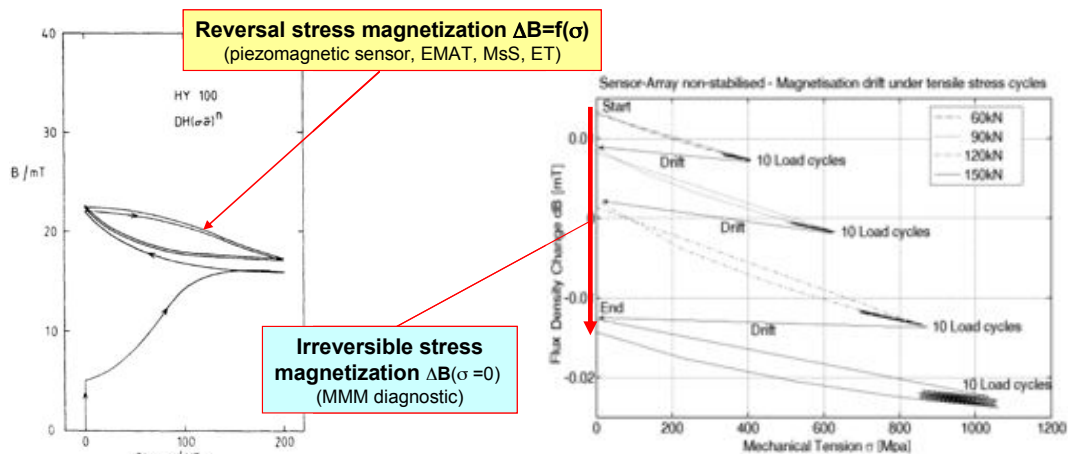
Magneto-mechanical effects (MME) are increasingly used to diagnose critical structural elements that are made of ferromagnetic and paramagnetic materials. In non-destructive testing (NDT) and systems to monitor early fatigue symptoms (structural health monitoring, SHM, prognosis health management, PHM), the following processes are used:

- reversible paraprocesses (Joule's effect, Villari effect and derivative phenomena),
- irreversible paraprocesses (ΔE effect, Metal Magnetic Memory (MMM), which is an equivalent of Natural Remanent Magnetization (NRM) in geophysics).

Diagnostic information not only about the level of the dislocation concentration (1st phase of fatigue) and cracks but also about changes in internal stresses and the history of maximal material effort can be obtained by means of non contact measuring of the magnetization level and distribution, Fig. 1. These features are the base for the Metal Magnetic Memory method.

The interpretation of the results to be used in the MMM method (research without artificial magnetization of metal) is difficult. The main problems are as follows:

- ❖ **natural magnetization signal** – the Earth's magnetic field is weak, its intensity and components are dependant on a place and time of performed research;
- ❖ **magnetization of the polycrystalline structure with different defects** – shortage of systematized knowledge on magnetic features of constructional steel, simplified models of magnetization without periodical components and noise of the Earth's magnetic field;
- ❖ **reference signal** – differential measurements applied in geophysical research and some MMM applications (increasing sensitivity of measurements), may not be applicable in the interiors with strong ferromagnetic objects (i.e. a palisade of the compressor/turbine blade).



a)

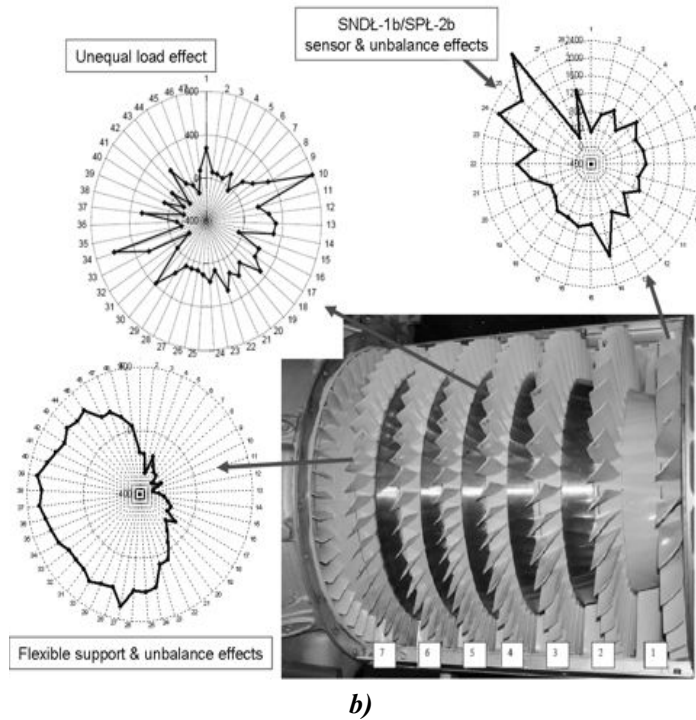


Fig. 1. Detection of stress prehistory: a) reversible and irreversible process of stress magnetization; b) identification of blade fatigue risk ($H_p = f(\text{blade number})$)

The numerical verified models of \mathbf{B}_{core} , $\mathbf{B}_{\text{crust}}$ and $\mathbf{B}_{\text{disturbance}}$ Earth's fields have been proposed to generate high-quality reference signals for the MMM expert systems (for NDT, SHM and PHM applications) and identify new diagnostic symptoms, as well as for the systematic/periodic calibration of the magnetic field sensors, taking the time of the testing and the location of the monitoring object into consideration. Verified models of the Earth's magnetism enable obtaining an accurate reference signal $\mathbf{B}_{m_ref} = \mathbf{B}_m \pm 5 \text{ nT}$.

In order to precisely determine the $\mathbf{B}_{\text{disturbance}}$ component for monitoring objects of significance located in Poland (applications of SHM and PHM with the use of the MMM method), the following data are anticipated to be used:

- reference data from ground-based observatories,
- correction data (RTK) from the system of ground-based reference observatories ASG EUPOS,
- converted data from SWPC NOAA.

Expected effects of the use of external reliable sources of data in MMM expert systems are as follows:

- an improvement in reliability and resolution of the \mathbf{B}_{m_ref} reference signal for a randomly chosen location for the monitored object;
- a capability to diagnose and predict regular and irregular geomagnetic phenomena in the vicinity of the monitored object.

(Research supervised by Mirosław Witoś, Air Force Institute of Technology, Warsaw).

3.3 X-ray Diffraction Measurements for Riveted Joints - the Application of a Novel Methodology

The X-ray diffraction method is the best, widely available, non-destructive measurement method used to determine the residual and load stresses in crystalline materials. This method can be applied without any limitations to flat specimens. Depending on the equipment geometry, the type of material and geometry of the specimen, there are many limitations, restrictions and recommendations which have to be fulfilled to obtain reliable results. This was the reason for working out a methodology for X-ray diffraction stress measurements for riveted specimens.

The first case to analyze is the necessity of choosing an X-ray tube suitable for the specimen material which will give the diffraction peaks in the range of 2θ angles between 120° and 180° . Afterwards it is crucial to make the best selection of Bragg's angle 2θ . In the vast majority of cases the best selection is the possibly biggest 2θ angle because of the best accuracy of the measurement. However, for example for aluminum alloys (for $\text{Cr}_{K\alpha}$ radiation), this choice is not so obvious. It is much more convenient to perform measurements not for the highest diffraction angle. The best selection in this case is $2\theta = 139,3^\circ$, and not $156,7^\circ$. Other selections which are necessary to be made before measurements are the collimator diameter, time of exposure, ψ tilts and ϕ oscillations. The proper selection of these parameters is crucial for the fast and efficient performing of measurements and for obtaining reliable results.

Before performing the measurement, especially in the case of the specimen with complicated geometry (for example in the case of riveted specimens made of aluminum alloys), it is necessary to analyze the results obtained paying special attention to the possibility of the appearing of the rivet head/driven rivet head shadow during the measurement. The work focused on differences between the X-ray stress measurement results obtained without any interference and the results received after eliminating the selected diffraction peaks for which the shadow of rivet head/driven rivet head has appeared.

The measurements programme performed under the Eureka IMPERJA project was concluded with the following observations:

- a well-rounded methodology is necessary to perform reliable and effective X-ray stress measurements,
- stress values in two directions (radial and tangential), in the riveted specimen, were obtained during the work – the obtained values are good introduction to stricter stress gradient measurements,
- it can be seen that stress measurements on the side of the driven rivet head are much more complicated than those on the side of the manufactured rivet head because of the shadow problem – careful analysis is necessary to introduce suitable corrections.

(Research supervised by Elżbieta Gadalińska, Institute of Aviation, Warsaw).

4. JOINTS

4.1 Investigations into the Durability of Epoxy-Bonded Joints

Bonded joints fulfill a significant role in the development of new technologies, particularly in the aerospace industry where they give new possibilities of connecting structural elements. With the adhesive connections, the construction size can be reduced and the airframe structure can be simplified. The bonded joints allow for reducing the aircraft operations costs by performing repairs of damaged parts instead of exchanging them. The Composite Patch Bonded Repair (CPBR) is a method that can be used for repairing the metallic and composite structures. The CPBR method includes the following steps: surface preparation prior to bonding, the imposition of Composite Patch, a cure cycle of the composite (prepreg) and the adhesive film, and the final treatment.

The most common techniques used for the surface preparation are Forest Product Laboratory's (FPL) technique and Phosphoric Acid Anodizing (PAA). Both methods ensure very good adhesion but they have some disadvantages. They require the application of toxic and aggressive acids, dangerous for the operator. Also, the use of acids for cleaning the surfaces can cause corrosion.

The sandblasting treatment of metal surfaces ensures quite good adhesion. This technique requires neither specialist equipment nor the use of toxic substances. Recommended by the Royal Australian Air Force (RAAF) the technique is also used by the Air Force Institute of Technology.

Sol Gel is a new product developed for the treatment of metal surfaces before bonding. It is not hazardous for the operator and it does not cause corrosion due to its specific chemical composition.

The properties of the adhesive film depend on the cure cycle parameters. The best mechanical properties are achieved when the cure cycle is performed in accordance with the material data sheet. However, the CPBR cure cycle of the recovery package – the film adhesive and the prepreg - should be performed in one operation. It is unacceptable to shorten the prepreg heating time to make it correspond to the cure cycle of the adhesive layer, since unhardened resin doesn't have desired mechanical properties. It is necessary to prolong the adhesive film cure cycle and perform it in accordance with the recommendations of the prepreg data sheet (Fig. 1).

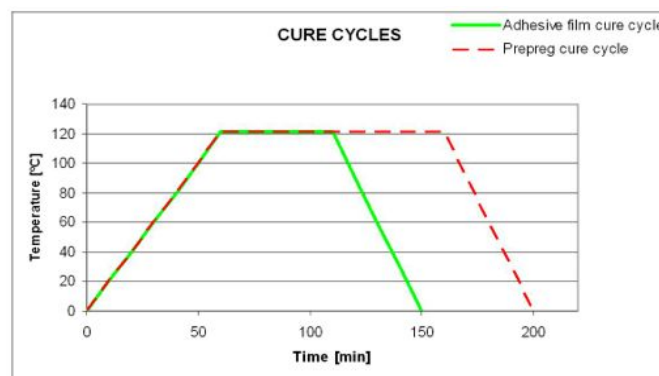


Fig. 1. Matching the cure cycle of the bonded layer to the prepreg required cure cycle

In order to determine:

- the influence of the preparation of the composite specimen's surface for bonding, and
- the effect of prolonged cure cycle time on the mechanical properties of the epoxy bonded layer

on the mechanical properties of the epoxy bonded layer, some tests were performed at the Air Force Institute of Technology.

Cure Cycle Time

The metal surface was covered with an adhesive film and with another piece of metal sheet. Two panels were made: the first was subjected to a cure cycle according to adhesive film data sheet – heating in 121°C for 60 minutes, the second was subjected to a prolonged cure cycle according to the repair prepreg data sheet - heating in 121°C for 105 minutes. Subsequently, the samples for testing were cut from these panels.

Both specimens have been tested to determine the forces separating the bonded joint and shear strength of the epoxy bonded layer.



Fig. 2. Specimen during the wedge test

The wedge tests were performed using the MTS 810.23 testing machine in accordance with ASTM D3762-03 (Fig. 2) at a constant displacement speed of 10 mm/min.

The presented research showed that the cure cycle time had little influence on shear strength and values of separating force, hence the adhesive film cure cycle may be extended and adapted to the prepreg cure cycle so that the cure cycles of prepreg and of the adhesive film can be carried out in one operation. This allows for performing damage repair using the Composite Path Bonded Repair method.

Preparation for Bonding

The preparation of the composite specimen's surface for bonding consists of its thorough cleansing and, optionally, increasing the contact surface by roughening. After a layer of the adhesive film has been applied and subjected to a heating cycle (cure cycle), there occurs diffusion of the adhesive into the composite along with the polymerization of the adhesive film molecules as well as the bonded composite and the adhesive.

The comparative environmental investigations into the influence of low temperature and high humidity on the durability of bonded joints made using the standard surface preparation method including sandblasting, and the Sol Gel preparation method were performed according to the “ASTM D3762 - 03(2010) Standard Test Method for Adhesive-Bonded Surface Durability of Aluminum (Wedge Test)”.

The tests showed that the bonded joint manufactured after surface preparation with Sol-Gel exhibits better durability in the Wedge Test. The average gain in durability is ~7%. Use of better adhesive films for the Sol Gel technique is likely to further improve the durability of the bonded joint.

(Research supervised by Michał Salaciński, Air Force Institute of Technology, Warsaw).

4.2 The Influence of the Degree of the Rivet Hole Sizing on the Fatigue Life

Rivet holes may be subjected to treatments that enhance their resistance to fatigue cracking. The most important operations include reaming and sizing. Reaming results in less diameter scatter and smoother holes. Compressive stresses are inserted into the inner layers of the material by sizing. These stresses hinder the formation of the hole's surface fatigue cracks.

Sizing of the holes can be made using special burnishing heads. This technology cannot be used for sizing the holes with diameters smaller than 3 mm. These holes can be sized by using a mandrel with an appropriate diameter. The resulting degree of deformation of the hole's surface depends on the difference between the diameter of the drilled hole and the sizing mandrel diameter.

The aim of this work was to analyse the course of the rivet hole sizing process using sizing mandrels and to evaluate the impact of the rivet hole sizing degree on the fatigue life. The research performed concerned improvement of the fatigue life of riveted joints as a result of local strain hardening of the rivet hole by the sizing process, which also results in improving the hole surface smoothness.

Experimental analyses of the sizing process and numerical simulations of the sizing were performed using ABAQUS FEM software. The analyses were extended by the statistical analyses of the experimental results.

Sizing and fatigue tests were performed in the Department Laboratory for Research on Materials and Structures (certified by the Polish Centre for Accreditation – PCA AB 372) of the Faculty of Mechanical Engineering at the University of Technology and Life Sciences in Bydgoszcz, using the testing machine INSTRON 8501.

Samples for tests were made of 1.27 mm thick non-clad plates of aluminium grade 2024-T3. Rivet holes were prepared assuming that they shall be used for 3 mm nominal diameter snap head solid rivets for aviation-related purposes. Finished holes for such rivets should be of 3.1 mm diameter with positive tolerance of +0,1 mm. Holes of such a diameter were obtained by two operations. The first one was drilling the hole and the second one – sizing the hole to the diameter of 3.1 mm. Samples with holes made in the conventional way (drilling or drilling and reaming) were also prepared for comparison purposes.

The samples with holes of different sizing degree were subject to fatigue tests. The tests were performed under zero-tension cycle conditions (cycle asymmetry factor $R=0$) with load frequency of 5 Hz. The tests were performed for three levels of a maximum load of the cycle $S_{max} = 150, 175$ and 200 MPa (three samples for each load level).

Fatigue life of riveted joints improves thanks to additional preparatory operations performed prior to riveting, such as hole sizing. Results obtained in this research confirm the positive effect of hole sizing on fatigue life. Cold work and polishing of the hole's surface by the sizing mandrel hinders initiation of micro-cracks. It should be emphasized that a number of factors influence fatigue life of the sample with riveted holes.

The results of this work indicate that just the hole surface polishing by reaming or low degree sizing improves fatigue life. The optimal value of sizing degree is $k = 3\div 5\%$ – higher value of sizing degree effectiveness in increase of the statistical dispersion of fatigue life.

(Research supervised by Adam Lipski, University of Technology and Life Sciences, Bydgoszcz).

4.3 Numerical Analysis of Material and Manufacturing Factors in Riveted Joints under the IMPERJA Project

The aim of the project was to improve fatigue performance of riveted joints in airframes. Fatigue strength of a joint depends on structural, material and manufacturing factors. The project involved numerical and experimental analysis of material factors and manufacturing imperfections.

The aim of the investigation was to evaluate the material properties of 2024T3 aluminium alloy subjected to various treatments (i.e. cladding, rolling direction). The strength of cladded sheets is about 7% lower than that of the bare ones (it is strictly joint with cladding layer thickness). The influence of the rolling direction on yield and limit stresses is about 5-6% in the case of bare sheets (specimens loaded in the rolling direction are stronger), whereas for cladded material the difference is lower than 2%.

The strain fields were detected with the Aramis system. It is an optical system for non-contact measurement of 3D deformations and strains in materials and structures during loading. The area of maximum/high plastic deformations, which was placed in the angle of 60° to the specimen axis, moved along the specimen and material separation occurred in this area.

The analysis of 2024T3 alloy structure was performed. In the elastic area, the regular crystals and frequent inclusions (i.e. iron inclusion phases) were observed. During the tensile loading the crystals were also stretched. Then a micro crack may be initiated at the inclusion particles and then voids grow around it.

The effect of a material model on the results of the numerical simulation of a tensile loaded sample with a hole was investigated. The application of Gurson's material model (with void nucleation) allows for determination of the sheet rupture as the moment when constraint force decreases to zero (material separation occurs), whereas for standard elasto-plastic material the criterion of failure can be defined as either strain (plastic strain) or stress dependent. Gradual material separation during loading can be observed using strain fields as well as principal stress fields.

Additionally, necking of the sheet cross section can be correctly determined only if Gurson's model is applied. Otherwise (for standard elasto-plastic material), the cross section decreases to zero.

(Research supervised by Elżbieta Szymczyk, Military University of Technology, Warsaw).

4.4 Riveted Lap Joints in Aircraft Fuselage. Design, Analysis and Properties Springer, 2012

Andrzej Skorupa, Małgorzata Skorupa (AGH University of Science and Technology, Krakow)

The major topic of the present book is fatigue of riveted lap joints representative for the pressurized aircraft fuselage. The book comprises 332 pages and addresses 232 references which include reports, papers and doctoral theses. The material presented is richly illustrated with 269 figures. An index including 230 entries facilitates tracking down of specific issues covered in the book.

The book is divided into 10 chapters and the most important issues of each chapter are recapitulated in the last section. Chapter 1 gives basic information on structural design solutions for fuselage skin joints and the loading conditions. Although the stress distribution in a fuselage lap joint is of a complex character, a great majority of experimental studies reported in the literature were carried out in laboratory conditions on simple small lap joint specimens under uniaxial tension. The relevance of such results to riveted joints in a real structure is considered in Chapter 2. The fatigue behavior of riveted lap joints shows a considerable dependency on factors associated with the production process. In Chapter 3, the following production variables are taken into account: sheet material, rivet type and material, as well as the manufacturing process, including the riveting technique, rivet hole imperfections, surface treatment of the sheets and the squeeze force. The latter is a major factor that influences the fatigue behavior of riveted joints. In Chapter 4, the dependence of the joint fatigue performance on various design parameters is addressed. Specifically, the effects of the number of rivet rows, rivet row spacing, rivet pitch in a row, rivet pattern, and sheet thickness are accounted for. An analytical solution and experimental results on load transmission in lap joints with mechanical fasteners are considered in Chapter 5. Special attention is paid to the experimental and theoretical determination of fastener flexibility and to friction between the faying sheets in view of their importance for load transfer. Eccentricities occurring in the overlap region of a joint induce the so-called secondary bending. Estimates of secondary bending by means of simple analytical models, FE computations and measurements are presented in Chapter 6. Also, implications of secondary bending for the joint fatigue performance are considered. The nucleation and shape development of fatigue cracks in longitudinal lap joints is covered in Chapter 7. Issues of special attention are the influence of the squeeze force on the mode of failure and the significance of fretting for fatigue crack initiation. A characteristic and very dangerous form of fatigue damage in longitudinal riveted lap joints is the so-called multi-site damage (MSD). In Chapter 8, passenger aircraft catastrophic accidents due to MSD are described first. Next, an overview of experimental investigations into MSD performed on full scale fuselage panels and riveted lap joint specimens is offered. Chapter 9 is devoted to fatigue crack growth and fatigue life prediction methodology for riveted lap joints including the MSD situation. Models and codes most commonly used for that purpose are outlined and stress intensity factor solutions appropriate for cracks at rivet holes are presented. A particular consideration is given to the equivalent initial flaw size concept due to its significance for the prediction quality. Residual strength predictions for riveted lap joints in a fuselage structure are addressed in Chapter 10. Failure criteria and crack growth directional criteria are thoroughly considered. Various computational approaches to estimate residual strength of flat and curved panels with riveted connections are presented and reported comparisons between predictions and experimental results are reviewed. Structural risk analysis methodology suitable to account for MSD crack growth in lap joints with mechanical fasteners is also addressed.

Recently, a favorable review of the book was produced in the International Journal of Fatigue by Prof. Jaap Schijve (<http://dx.doi.org/10.1016/j.ijfatigue.2013.02.001>) who writes: “Whenever fatigue of lap joints must be considered for designing a fuselage or analyzing fatigue in lap joints of existing aircraft, this book should be consulted. There is no comparable book with such a comprehensive and explanatory description of fatigue of riveted lap joint.”

4.5 Experimental and Numerical Analysis of the Rivet Installation Process

Bulletin of the Military Technical Academy (Biuletyn WAT), 2013, in print (in Polish)
A. Korbel, E. Szymczyk, A. Skorupa

Installation a 5 mm dia, round head rivet from the AD material to connect two 1.9 mm thick sheets from the D16 Al alloy was investigated experimentally and numerically employing the FE method.

The dependency of the rivet driven head dimensions and of radial expansion of the rivet hole on the rivet squeeze force level was determined experimentally. The hole expansion measurements indicated that increasing the rivet squeeze force yielded larger hole expansion, Fig. 1. Hole expansion was observed to vary along the thickness of the joint showing the smallest value on the faying surface of the sheets and the largest value under the rivet driven head.

The FE analyses were carried out using the MSC Marc software capable of accounting for strongly non-linear material behaviour due to large displacements and plastic strains. The components of the joint were described using 3D models, Fig. 2. Two different isotropic elastic-plastic characteristics of the rivet material and of the sheet material were considered in the FE analyses, namely a step-wise linear curve that fits experimentally obtained true stress-true strain data (O-L model) and the Johnson-Cook equation (J-C model). Comparisons between the computed and observed effect of the squeeze force on the rivet driven head dimensions and on hole expansion revealed that though the O-L model correlates the measured constitutive behaviour, the J-C model leads to a better agreement between the FE and experimental results, Fig. 1. This implies that in order to adequately reflect in numerical analyses the influence of the riveting process, an appropriate adjusting of the material constitutive response may be needed.

In addition, numerical results on the effect of the squeeze force on residual stresses in the rivet hole vicinity have been produced. For a high squeeze force value, compressive circumferential stresses occur along the whole thickness of the joint, whilst for a low squeeze force, such stresses are generated only in the sheet next to the rivet driven head. Further, the analyses indicate that compressive radial residual stresses at the rivet hole and their area increase with increase with the squeeze force value.

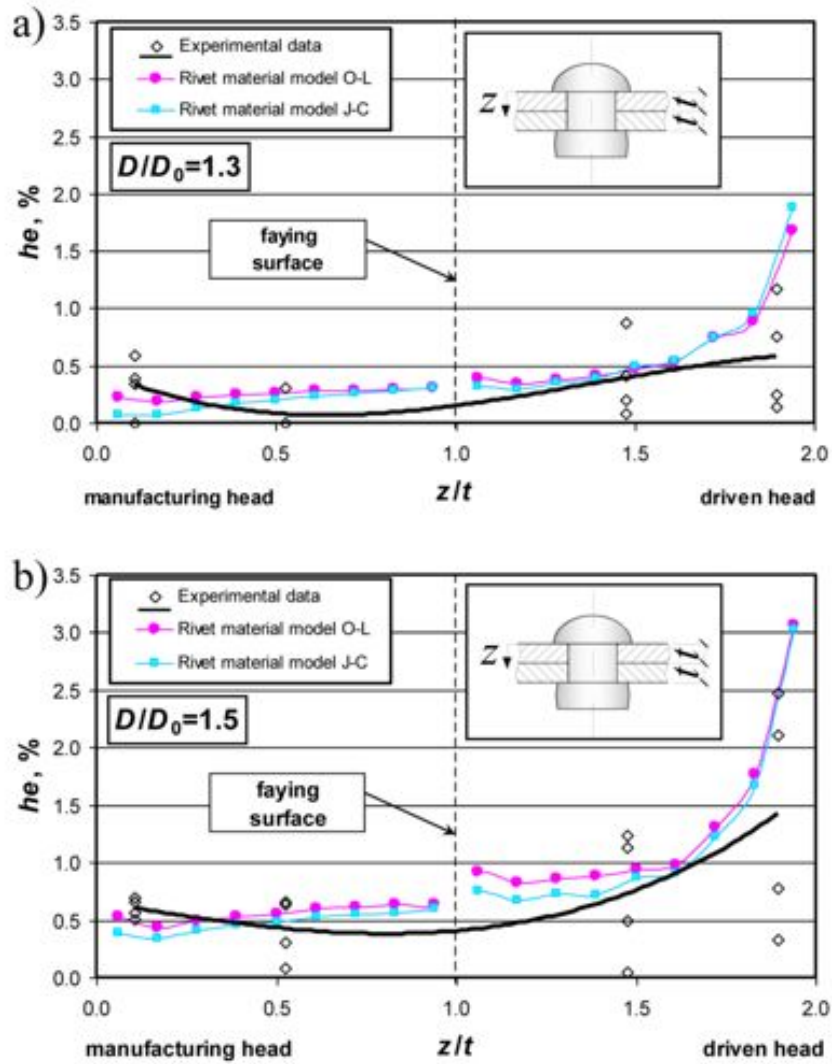


Fig. 1. Comparisons between measured and computed for two different rivet material models rivet hole expansion two squeeze force values corresponding to: (a) $D/D_0=1.3$; (b) $D/D_0=1.5$. D - rivet driven head diameter, D_0 - rivet shank diameter

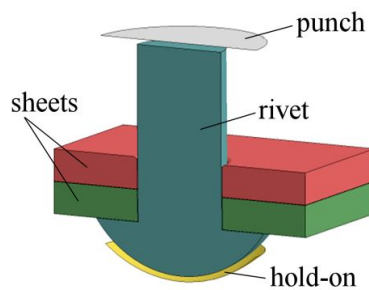


Fig. 2. Modelling of rivet and sheets in the FE analyses

4.6 Fatigue Crack Location and fatigue life for riveted lap joints in aircraft fuselage

Int J Fatigue (2013), <http://dx.doi.org/10.1016/j.ijfatigue.2013.01.01>

A. Skorupa, M. Skorupa, T. Machniewicz, A. Korbel
and

4.7 An Experimental Investigation on Crack Paths and Fatigue Behaviour of Riveted Lap Joints in Aircraft Fuselage

Proc. of the 4-th International Conference on Crack Paths (CP 2012), Gaeta, Italy, Sept. 2012

A. Skorupa, M. Skorupa, T. Machniewicz, A. Korbel

Effects of variables related to design and production of riveted lap joints representative of longitudinal sheet connections for a pressurized transport aircraft fuselage were experimentally investigated. Three-row riveted lap joint specimens were used for fatigue tests. The rivet row spacing and the rivet pitch in row were equal to $5d$ (d – rivet diameter), as typical for fuselage skin connections. The rivet holes were drilled according to the process specification of the Polish aircraft industry. The sheet material was the D16CzATW aluminium alloy which is a Russian equivalent of the western 2024-T3 Alclad alloy. The sheets of three different thicknesses (1.9, 1.2 and 0.8 mm) were assembled using two types of protruding head rivets differing in the manufactured head geometry, namely with a round head and with a so-called compensator, Fig. 1. The compensator, which is a small protrusion on the mushroom rivet head, yields increased rivet hole expansion in the adjacent sheet. The rivet material was the P24 Al alloy equivalent to the western 2117-T3 material used for the AD rivets. The rivets were installed under load control to produce ratios of the rivet driven head diameter to the rivet shank diameter (D/d) ranging between 1.3 and 1.6. Such a range is typical for the aircraft industry practice.

The rivet installation causes rivet hole expansion, which generates compressive residual tangential stresses in the hole vicinity. The higher the squeeze force level, the larger the compressive tangential stress area, which affects the initiation location and path of fatigue cracks at rivet holes and the joint fatigue life. Increasing squeeze force yields also a higher residual clamping between the sheets beneath the rivet heads. This leads to transmitting a portion of the applied load by friction, which again can influence a mode of joint failure.

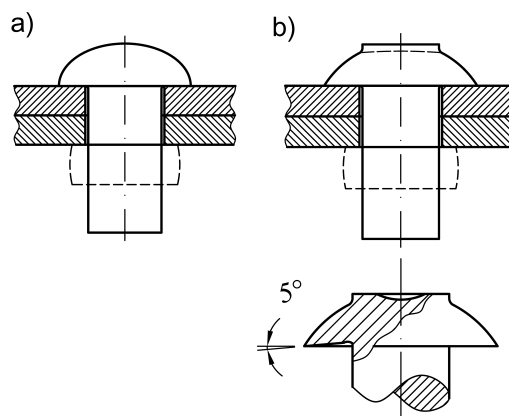


Fig. 1. Rivet types used in the experiments: (a) round head rivet; (b) rivet with the compensator

In order to investigate the effect of squeeze force on the lap joint fatigue performance measurements of hole expansion and load transfer were performed. Hole expansion was defined as $he = [(d_e - d_o) / d_o] 100\%$, where d_o and d_e are the rivet hole diameter prior to riveting

and the expanded rivet hole diameter respectively. A new technique of hole expansion measurements was developed. Both rivet heads were first cut away. Then for either sheet a 0.1 to 0.2 mm thick layer of the material was removed by milling. The machined area was subsequently polished to facilitate observations of the rivet/hole boundary and the d_e diameter was determined as the average from diameter measurements in several directions. The milling and polishing operation was then repeated for either sheet to obtain d_e at a location of mid-thickness of the sheet. Only connections of the 1.9 mm and 1.2 mm thick sheets were considered. For the round head rivets hole expansion was always larger in the sheet adjacent to the rivet driven head, contrary to the rivets with compensator for which expansion was larger in the outer sheet.

Also load transfer measurements using strain gauges were carried out for the joints from 1.9 mm thick sheets and round head rivets. Two D/d ratios, namely of 1.3 and 1.5 were taken into account. The results are shown in Fig. 2. It is seen that for the lower squeeze force ($D/d=1.3$) a non-symmetrical load transmission by the outer rows occurred and load transmission by the middle row is considerably lower than by the outer rows. For the larger squeeze force load transmission by all rivet rows is more uniform, which leads to a lower bearing load in the critical outer rows.

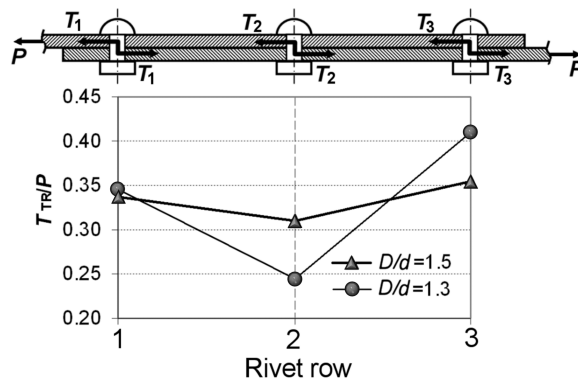


Fig. 2. Effect of a squeeze force on load transmission for joints from 1.9 mm thick sheets and round head rivets

All riveted specimens were tested under constant amplitude loading at a frequency of about 20 Hz with the stress ratio of 0.1. Three maximum stress values, $S_{max}=120, 100$ and 90 MPa, were applied. The loading conditions simulated hoop stress variations due to cabin pressurization. Fractography indicated that in all specimens fatigue cracks always initiated in one of the end rivet rows (in few cases in both rows) on the faying surface of the loaded sheets, where a combination of tensile stresses contributed by the axial forces and by the secondary bending moments obtains its maximum. Due to stress concentration the cracks nucleated at or close to the rivet holes. Usually multiple site damage occurred. Crack initiation and growth prior to the occurrence of a visible crack consumed the major part of the fatigue life. The period from a first crack link-up to failure typically took only a few percent of the total joint endurance.

The effect of the squeeze force value on the crack initiation location, crack shape and crack trajectory was strongly dependent on a specific combination of the sheet thickness and rivet type. For joints from the thicker sheets (1.9 and 1.2 mm) all observed trends could be rationalized by considering interactions between applied loading and effects of the riveting process, represented by the hole expansion behaviour and load transfer distribution. In the case of thin sheets, riveting imperfections could have a profound influence on the joint fatigue performance.

For joints with the round head rivets increasing the rivet squeeze force yielded always a longer fatigue life of a joint, as shown in Fig. 3. This figure also indicates that a trend of increase in the joint fatigue life with reducing sheet thickness, expected from secondary bending arguments, was not fully systematic due to riveting imperfections inherent in riveted joints from thin sheets.

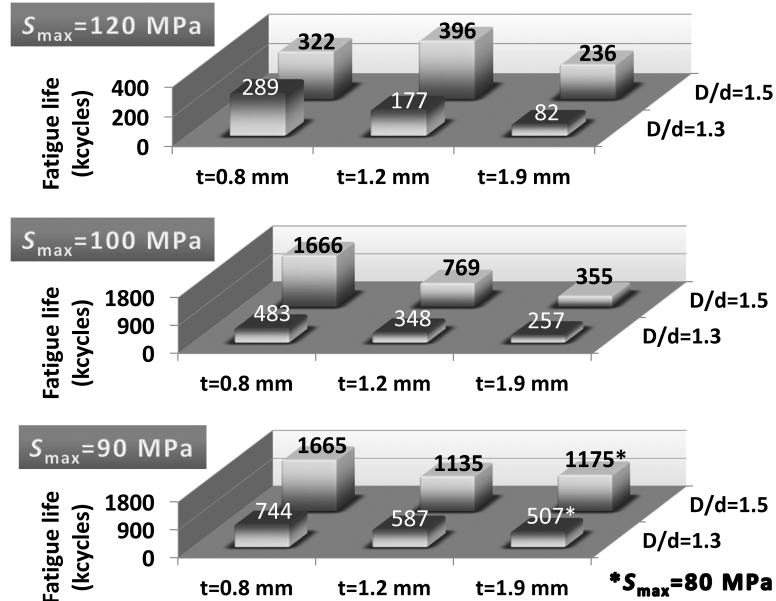


Fig. 3. Effect of a squeeze force and sheet thickness on fatigue life of joints with round head rivets

Application of the rivets with compensator was beneficial only in the case of lap joints from thicker sheets (1.9 and 1.2 mm). For a given D/d ratio, fatigue lives of specimens from 1.9 mm thick sheets assembled using the rivets of this type observed at $S_{max}=120$ and 100 MPa were higher by 40 to 90% than in the case when the round head rivets were used. Applying the rivets with compensator to connect thin sheets brought no benefits compared to the round head rivets because, due to a specific shape of the manufactured head bottom surface, significant local imperfections of the sheet beneath that rivet head precipitated failure.

4.8 Analysis of the Quasi-Static Riveting Process for 90° Countersunk Rivet

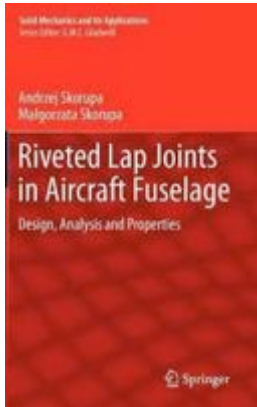
Squeezing force and a rivet type influence directly stress and strain fields around the rivets generated during the riveting. Compressive stresses prevent crack nucleation, which extends fatigue life of joints. Determination of stress and strain pattern around the rivet for various rivet types and riveting parameters was an important part of the IMPERJA project, which was devoted to improvement of fatigue life of riveted joints in aircraft structures. This work was devoted to experimental and numerical investigations into the stress and strain state during the riveting process. This state has crucial influence on the fatigue performance of riveted joints. The analyses and FEM calculations were performed for countersunk solid rivets with strain gauges. Five characteristic moments of the riveting process were distinguished. The reversal strain signal during the riveting process was recorded in the measurements. This phenomenon was not observed in numerical calculations. The working hypothesis was assumed that between the rivet and sheets cold welding joints were formed and destroyed during the riveting process, which resulted in reversal strain signal. This phenomenon was not represented in the calculations. The numerical analysis of contact normal stresses between the rivet and sheets showed that in some regions stresses exceeded the level necessary for joint formation of this type. Further research is necessary to confirm the existence of cold welding joints as a result of the riveting process.

(Research supervised by Wojciech Wronicz, Institute of Aviation, Warsaw).

5. IMPORTANT PUBLICATIONS



springer.com



“Riveted Lap Joints in Aircraft Fuselage”

Design, Analysis and Properties

Andrzej Skorupa and Małgorzata Skorupa,
AGH University of Science and Technology, Krakow, Poland

- ▶ Provides help in rational planning of experiments on riveted lap joints in aircraft fuselage
- ▶ Provides essential information for safe in-service operation of aircrafts
- ▶ Includes 200 figures

Fatigue of the pressurized fuselages of transport aircraft is a significant problem all builders and users of aircraft have to cope with for reasons associated with assuring a sufficient lifetime and safety, and formulating adequate inspection procedures. These aspects are all addressed in various formal protocols for creating and maintaining airworthiness, including damage tolerance considerations. In most transport aircraft, fatigue occurs in lap joints, sometimes leading to circumstances that threaten safety in critical ways. The problem of fatigue of lap joints has been considerably enlarged by the goal of extending aircraft lifetimes. Fatigue of riveted lap joints between aluminum alloy sheets, typical of the pressurized aircraft fuselage, is the major topic of the present book. The richly illustrated structural design solutions and loading conditions for fuselage skin joints; relevance of laboratory test results for simple lap joint specimens to riveted joints in a real structure; effect of various production and design related variables on the riveted joint fatigue behavior; analytical and experimental results on load transmission in mechanically fastened lap joints; theoretical and experimental analysis of secondary bending and its implications for riveted joint fatigue performance; nucleation and shape development of fatigue cracks in riveted longitudinal lap joints; overview of experimental investigations into the multi-site damage for full scale fuselage panels and riveted lap joint specimens; fatigue crack growth and fatigue life prediction methodology for riveted lap joints; residual strength predictions for riveted lap joints in a fuselage structure. The major issues of each chapter are recapitulated in the last section.

“Good Practice for Fatigue Crack Growth Curves Description”

Sylwester Kłysz¹ and Andrzej Leski²

^[1] Air Force Institute of Technology, Warsaw, Poland and University of Warmia and Mazury, Olsztyn, Poland

^[2] Air Force Institute of Technology, Warsaw, Poland

<http://www.intechopen.com/books/applied-fracture-mechanics/good-practice-for-fatigue-crack-growth-curves-description>



in “Applied Fracture Mechanics”

Edited by Alexander Belov, ISBN 978-953-51-0897-9, Hard cover, 378 pages, Publisher: InTech, Chapters published December 12, 2012 under CC BY 3.0 license DOI: 10.5772/2823



“Fatigue of Aircraft Structures”

Antoni Niepokólczycki (Editor)

Institute of Aviation, Warsaw, Poland

<http://versita.com/fasms/>

Once a year, this report gives information on recent works from the area of fatigue of aircraft structures.

The publication focuses on problems of aeronautical fatigue and structural integrity. The preferred topics include:

- full-scale fatigue testing of aircraft and aircraft structural components,
- fatigue of materials and structures,
- advanced materials and innovative structural concepts,
- damage tolerant design of aircraft structure,
- life extension and management of ageing fleets,
- structural health monitoring and loads,
- fatigue crack growth and life prediction methods,
- NDT inspections,
- airworthiness considerations.